REPORT OF THE LARGE SOLENOID DETECTOR GROUP[*]

G. G. Hanson

Stanford Linear Accelerator Center, Stanford University, Stanford, California 94305

S. Mori

Institute of Applied Physics, University of Tsukuba
Sakura-mura, Niihari-gun, Ibaraki 305, Japan

L. G. Pondrom

Physics Department, University of Wisconsin, Madison, Wisconsin 53706

H. H. Williams

Physics Department, University of Pennsylvania, Philadelphia, Pennsylvania 19104

B. Barnett
Johns Hopkins University

V. Barnes
Purdue University

R. Cashmore
Oxford University

M. Chiba
Tokyo Metropolitan University

R. DeSalvo
Cornell University

T. Devlin
Rutgers University

R. Diebold
U.S. Department of Energy

P. Estabrooks
Carleton University

S. Heppelmann
University of Minnesota

I. Hinchliffe
Lawrence Berkeley Laboratory

J. Huston
Michigan State University

T. Kirk
Fermi National Accelerator Laboratory

A. Lankford
Stanford Linear Accelerator Center

D. Marlow
Princeton University

D. Miller
Purdue University

P. Oddone
Lawrence Berkeley Laboratory

S. Parker
University of Hawaii

F. C. Porter
California Institute of Technology

N. Tamura
Kyoto University

D. Theriot
Fermi National Accelerator Laboratory

G. Trilling
Lawrence Berkeley Laboratory

R. Wigmans
NIKHEF, Amsterdam

N. Yamdagni
University of Stockholm

To appear in the Proceedings of the Workshop on Experiments, Detectors, and
Experimental Areas for the Supercollider, Berkeley, California, July 7–17, 1987

ABSTRACT

This report presents a conceptual design of a large solenoid detector for studying physics at the SSC. The parameters and nature of the detector have been chosen based on present estimates of what is required to allow the study of heavy quarks, supersymmetry, heavy Higgs particles, WW scattering at large invariant masses, new W and Z bosons, and very large momentum transfer parton-parton scattering. Simply stated, the goal is to obtain optimum detection and identification of electrons, muons, neutrinos, jets, W's and Z's over a large rapidity region. The primary region of interest extends over ± 3 units of rapidity, although the calorimetry must extend to ± 5.5 units if optimal missing energy resolution is to be obtained. A magnetic field was incorporated because of the importance of identifying the signs of the charges for both electrons and muons and because of the added possibility of identifying τ leptons and secondary vertices. In addition, the existence of a magnetic field may prove useful for studying new physics processes about which we currently have no knowledge. Since hermeticity of the calorimetry is extremely important, the entire central and endcap calorimeters were located inside the solenoid. This does not at the moment seem to produce significant problems (although many issues remain to be resolved) and in fact leads to a very effective muon detector in the central region.

1. Introduction

The main motivation for the SSC is the expectation that new physics in the form of new heavy particles, such as Higgs bosons, supersymmetric particles, heavy fermions, heavy W's or Z's, or composite particles, will be discovered in the TeV mass range. Such particles would be produced in the central rapidity region and would decay to high-p_T electrons, muons, or jets, often in events with large missing transverse energy (E_T) due to undetectable neutrinos.

The Large Solenoid Detector Group has studied a large 4π detector in a solenoidal magnetic field from two aspects:

1. Detector characteristics needed to look for the new physics

2. Improvements on the design of a large 4π solenoidal detector over previous designs [1–3].

Our large solenoid detector was conceived as being built with more-or-less "conventional" technology, although in practice such a detector would require a great deal of research and development to build, particularly for the calorimetry and electronics. Such a detector must be capable of operating at the SSC design luminosity of 10^{33} cm^{-2}s^{-1}. We also considered operation at lower and higher luminosities. The detector characteristics are dictated by the desire to detect and identify jets, electrons, muons, and neutrinos (via the missing momentum). Particular emphasis is placed on the identification of electrons and muons; backgrounds should be reduced to a level that is small compared to the rate for prompt real leptons. Since rates for interesting events will be small and the background processes complex, high priority was also given to the determination of the sign of the electric charge for both electrons and muons.

To accomplish electron identification and charge sign determination, tracking in the presence of a magnetic field is required in the inner volume surrounded by the calorimeter. In addition, there are many other motivations for tracking. Our summary of the most important reasons includes:

1. Identification of electrons.

2. Separation of multiple interactions within the same bunch crossing.

3. Matching electrons, muons, and jets to the correct vertex.

4. Electron charge sign determination.

5. Improving e/π separation.

6. Identification of secondary vertices.

7. Identification of τ leptons.

8. Invariant mass or momentum cuts.

9. Establishing the credibility of new physics and providing redundancy.

We note that items 4–9 require a magnetic field. While some of the items are of a higher priority than the others, we are convinced that a great deal of flexibility and power for addressing the physics issues is lost if a magnetic field is not incorporated.

There are additional arguments that may be given, e.g., that with a magnetic field one can verify calorimeter measurements and improve the hermeticity of the overall detector if it is not possible to build a "crackless" calorimeter. However, we do not give these arguments as large a weight since it is our goal to provide good charged particle tracking without compromising compensating and hermetic calorimetry.

2. Physics Requirements

We met with members of the Physics Parametrization Groups on Heavy Higgs, Intermediate Mass Higgs, Nonstandard Higgs, Supersymmetry, Heavy Quarks and Leptons, New W's and Z's, and Jets and Compositeness [4]. From these discussions and from the summary talks of these groups the physics requirements for detectors which will look for high-p_T physics at the SSC were determined. We should keep in mind that the new physics actually found at the SSC may be something other than what was expected. The Parametrization Groups provided models in terms of our present understanding of what physics the detectors should be able to deal with.

The basic requirements can be summarized as follows:

1. Electron and Muon Identification

   - $|\eta| < 2.5 - 3$ (5 for muons)
   - Sign of charge to $0.5 - 1$ TeV/c
   - $e, \mu/\pi$ rejection at least 10^{-3}
   - Mostly isolated tracks

2. Calorimetry

- Missing $E_T > 100$ GeV
- Hermeticity crucial!
- $|\eta| < 5.5$ ($\sim 0.5°$)
- Electromagnetic: $\sigma_E/E = (0.10 \text{ to } 0.15)/\sqrt{E} + 1\%$
- Hadronic: $\sigma_E/E = 0.50/\sqrt{E} + 2\%$
- Electromagnetic $\Delta\eta \times \Delta\phi$ segmentation: $0.02 \times 0.02 - 0.03 \times 0.03$
- Hadronic $\Delta\eta \times \Delta\phi$ segmentation: 0.06×0.06

3. Tracking

- $|\eta| < 2.5 - 3$
- $\sigma_{p_T}/p_T \sim 0.3 - 0.5\, p_T$ (TeV/c)
- Mostly isolated tracks
- Useful to check missing energy

4. Microvertex Detector

- Useful to tag b's and τ's

Probably the most difficult requirements to meet are those for an intermediate-mass Higgs decaying into $b\bar{b}$ or $\tau^+\tau^-$. For this physics one needs to tag b's or τ's using a microvertex detector at the design luminosity of 10^{33} cm^{-2}s^{-1}. In addition, this group wants to identify electrons in b jets.

3. Overview of Detector

In an effort to meet the physics requirements, we paid special attention to optimizing tracking and calorimetry together. The outer radius for tracking was reduced from the Snowmass 86 value in order to allow for at least 10 interaction lengths of hermetic compensating calorimetry entirely inside the magnet coil. In addition, we added intermediate tracking to cover $1.2 < |\eta| < 3$. The iron flux return was then available for use in the central muon detector. We discussed ways to optimize electron identification, possibly including transition radiation detectors, especially in the forward regions. We studied the measurement of muon momentum for muons in the central region by using only the bending angle measured just outside the coil and with central tracking included. We also discussed how such a large solenoid detector might operate at a high luminosity of 10^{34} cm^{-2}s^{-1}. The new design for a large solenoid detector is shown schematically in Figs. 1(a) and 2. Model A from the DCMAP report [2] is shown for comparison in Fig. 1(b). The new improved version has shrunk in outer radius from 10.5 m to 7.6 m. The detector components are described in detail in the following sections.
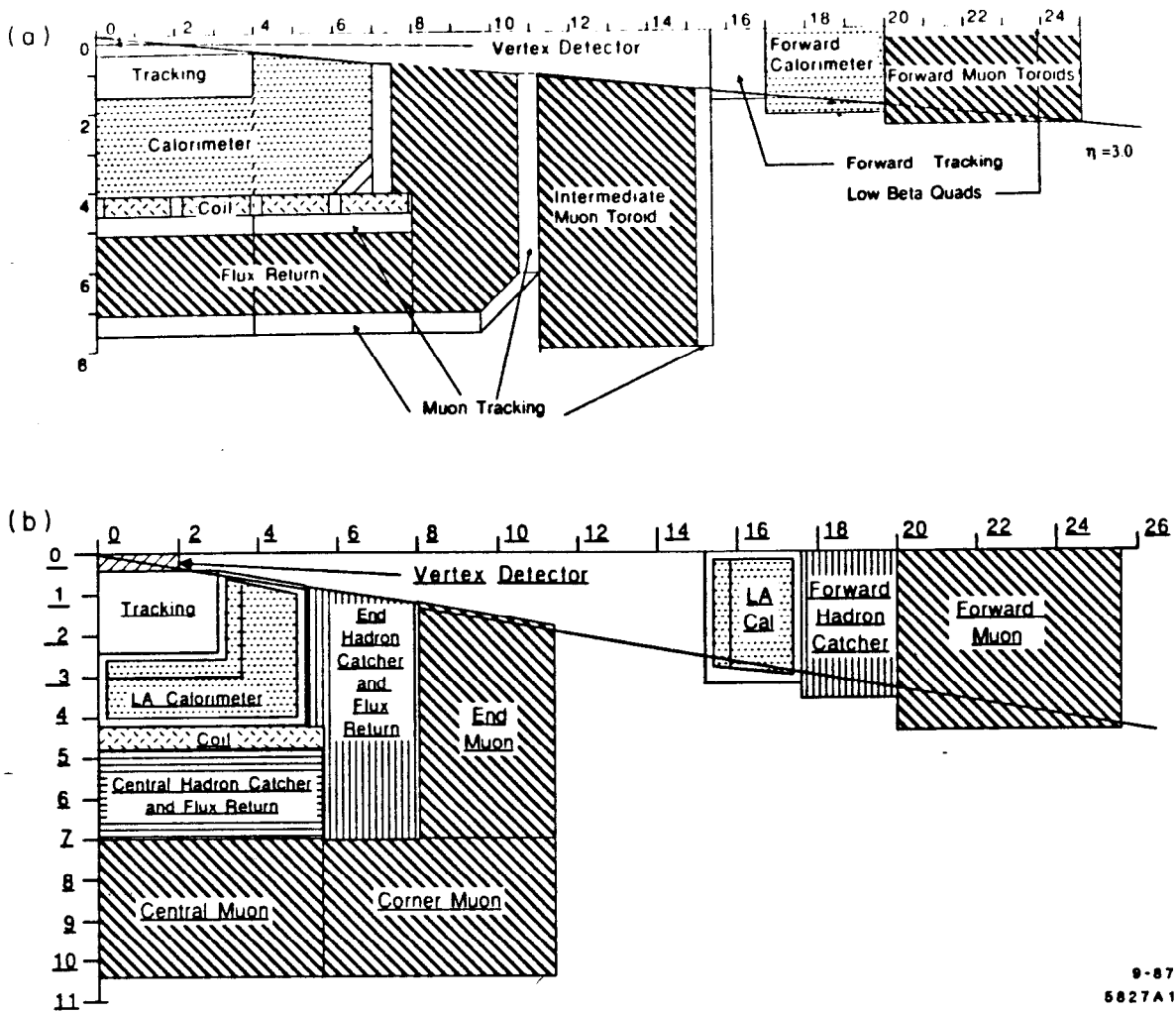
Fig. 1. (a) Schematic view of the Large Solenoid Detector. (b) Model A from Reference 2.

4. Magnet

The decision to locate all of the calorimetry inside the solenoid coil has profound consequences on the solenoid coil. The coil must be large (8.7 m × 16 m in this case) and must be able to carry a large weight inside the bore (5000 tons). However, restrictions on the thickness of the coil can be relaxed because the coil will no longer interfere with the energy measurement or affect the e/h signal ratio. Muon tracking chambers can be located just outside the coil because there is sufficient absorber to reduce the hadron shower. The flux return can now be utilized not only for flux return but for muon identification and a redundant momentum measurement of the muon as well.

4.1. Magnet Design

As is shown in Fig. 1(a), the coil extends from a radius of 4.1 m to 4.6 m. The magnetic field inside the coil is 2 Tesla providing over 8 Tesla-meters of magnetic analysis for exiting muons. The first layer of muon tracking chambers, extending from 4.6 m to 5.1 m, is just outside the coil. This tracking chamber is used to measure the angle of the exiting muon very accurately in order to be utilized as the p_T cutoff for the Level 1 muon trigger and as the primary momentum measurement for high energy (> 1 TeV/c) muons. The steel flux return, extending from 5.1 m to 7.1 m, is located outside the first layer of muon tracking chambers. The calculated magnetic field in this steel is 1.5 Tesla. The outer layer of muon tracking chambers, extending from 7.1 m to 7.6 m, is located outside the flux return. The angle measurement in this layer will be used in the Level 1 or Level 2 muon trigger to point back to the interaction vertex and as a redundant momentum measurement since the flux return has 3 Tesla-meters of magnetic analysis capability. An end view of the detector is shown in Fig. 2.
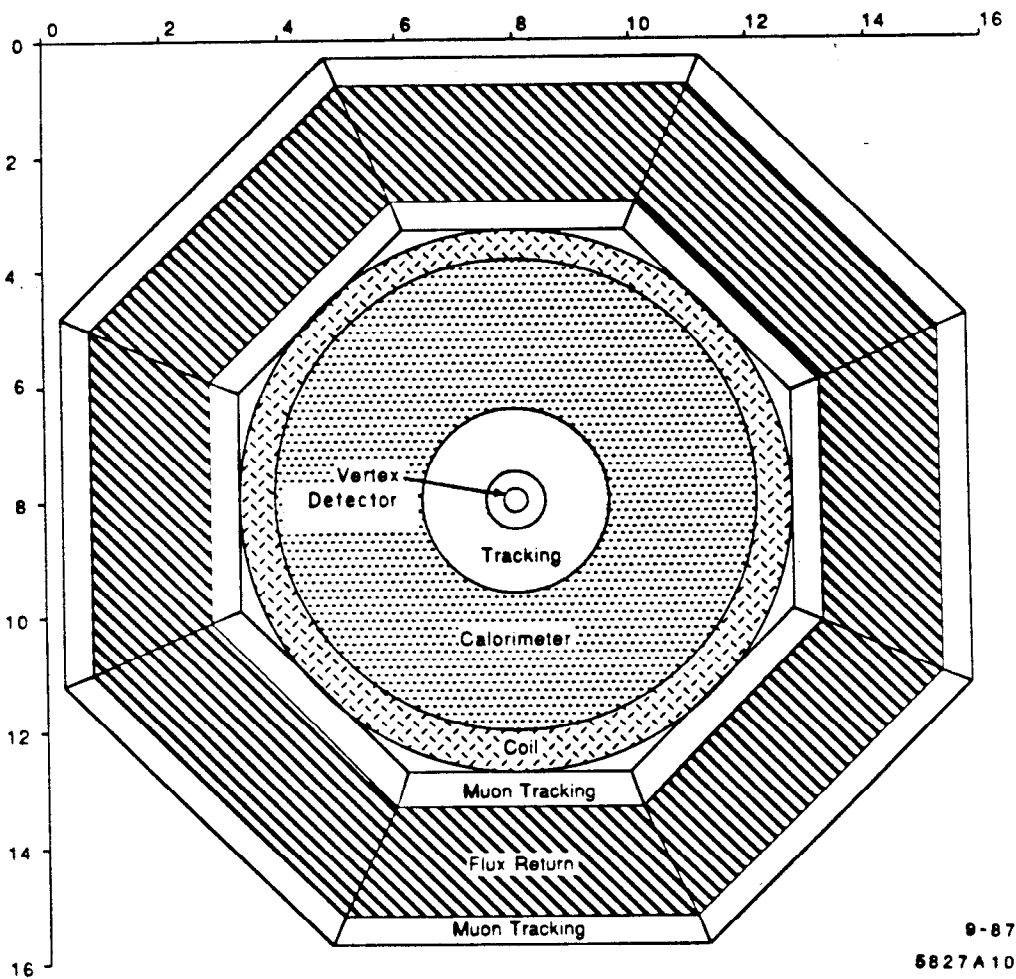

Fig. 2. End view of the Large Solenoid Detector.

The parameters of the solenoid are given in Table I. Because of the large size, it is proposed that the solenoid be constructed in several modules.

Table I. Main Parameters of the Super Solenoid

Bore Diameter	8.2 meters
Total Length	16 meters
Central Field	2 Tesla
Number of Modules	8
Free Space Between Adjacent Modules	0.34 meters
Total Stored Energy	1 GigaJoule
Overall Inductance	80 Henries
Total Weight	450×10^3 Kilograms

Another advantage of building the solenoid in several modules is that the free space between the separate modules can be used for support structure to carry the weight of the calorimeter and as an exit path for signal cables if necessary.

A cross section of one of the solenoid modules is shown in Fig. 3 and the parameters of the module are given in Table II.
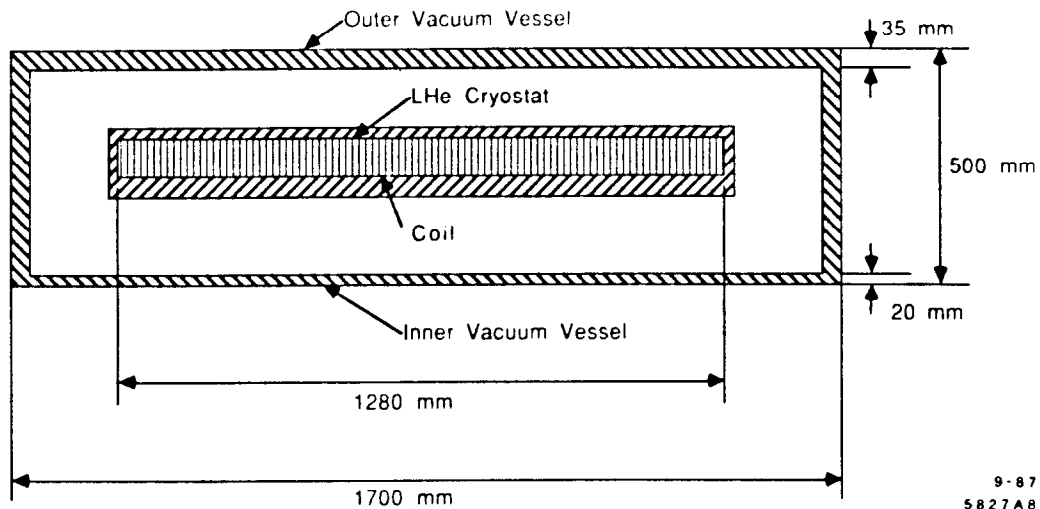

Fig. 3. Cross section of the solenoid module.

Table II. Parameters of the Solenoid Module

Length	1.7 m
Diameter (inner/outer)	8.2 m/9.2 m
Coil Length	1.28 m
Current	5000 A
Central Field	2.0 T
Winding	
Number of Layers	6
Total turns of winding	642
Stored Energy	125 MJ
Cryostat: He Vessel	
Material	SUS 304N
Wall Thickness (inner/outer)	3.5 cm/2.5 cm
Length	1.4 m
Conductor	AMY-type
Weight	56×10^3 Kg
Cold Mass	33×10^3 Kg
Temperature rise for 125 MJ	75°K from 4.2°K

Since the coil is now outside the calorimeter, one is no longer constrained to build a "thin" solenoid such as is currently used in CDF or the LEP detectors. A more conservative thick design is chosen. The conductor chosen here is the AMY-type conductor [5], cross section shown in Fig. 4 and parameters listed in Table III. The AMY conductor is made of hard copper and has an allowable stress of about 20 kg/mm². A stainless steel support structure can be used to reduce the conductor thickness. A detailed cross section of the liquid helium cryostat and the superconducting coil is shown in Fig. 5. The pool boiling method of cooling is used. Both the cryostat and vacuum chamber are made of stainless steel. The magnet is cryostable, but for safety reasons is designed to allow quenches to occur.

Table III. Parameters of the AMY Conductor

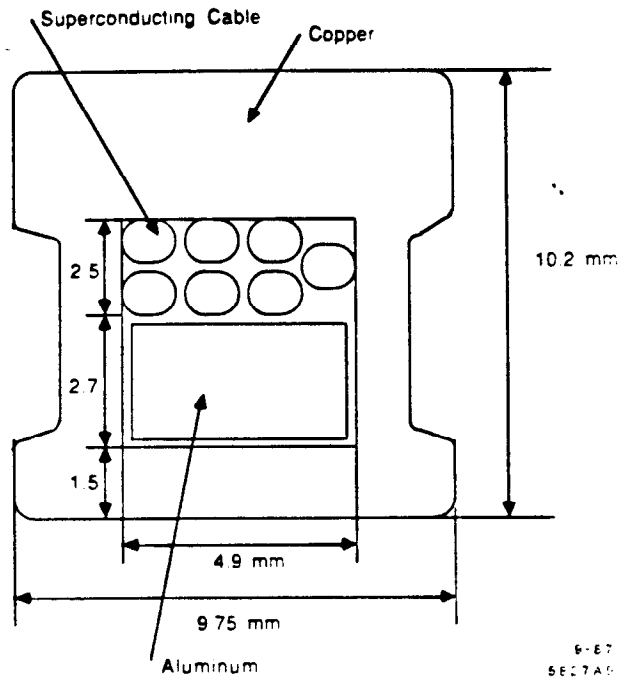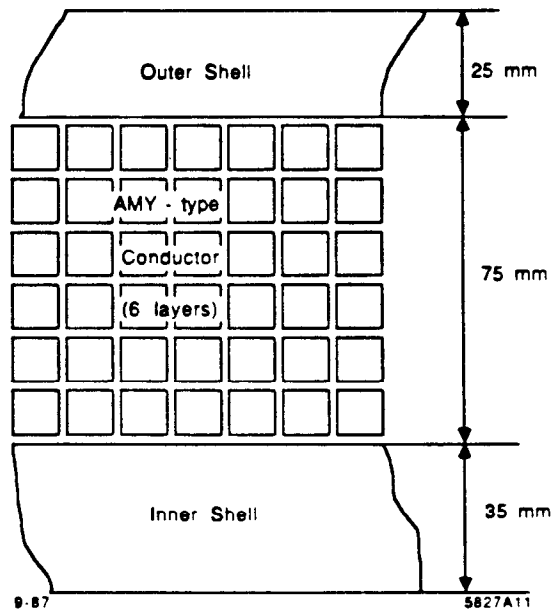|	
Superconductor	Nb-46.6 wt% Ti
Cross Section	9.8×10.2 mm²
Strand Diameter	1.35 mm
Number of Strands	7
Number of Filaments (30 μmø) per strand	1025
Critical Current:	
At 4.4 T (4.2°K)	11760 A
At 6.0 T (4.2°K)	8610 A

Fig. 4. Cross section of the AMY conductor.

Fig. 5. Cross section of the liquid helium cryostat
and superconducting coil.

4.2. Detector Assembly

A magnet this large is not assembled as a single object. Having already divided the coil into several modules, there is no reason not to divide the flux return as well. A possible cut is at $z = 4$ m and another at $z = 8$ m. The ring of the octagonal flux return is assembled as a single object, 4 m in length, 15 m wide and 15 m high. This forms the main structural element of the central detector and has a weight of almost 2500 metric tons. Two of the magnet modules are assembled together with additional structural support as a single unit having sufficient strength both to hold the modules themselves with their associated magnetic forces and to support the calorimeter which will subsequently be inserted. This unit is inserted into the flux return ring and literally hung from it by means of bolted connections which center the magnet modules, space them off the ring, and allow space for the muon tracking chambers. These connections will take up approximately half of the azimuthal area allowing the muon chambers to be inserted and aligned through the remaining gaps. This process is repeated four times to produce the entire barrel of the central detector. The two endcaps are solid steel and are assembled separately. The endcaps when assembled each weigh almost 3400 metric tons.

The central calorimeter meanwhile has been assembled as a separate object. The details of how this calorimeter is mated to the solenoid/flux return are dependent upon the calorimeter technology chosen. If the calorimeter is made of uranium-liquid argon, the number of cryostats would probably be kept to a minimum in order to minimize hermeticity problems. One possible choice is to cut it at 90°. This would give only two cryostats each weighing approximately 2500 tons. Each cryostat would be mated to two of the solenoid/flux return rings. If the calorimeter is made with either lead-scintillating fiber technology or lead-TMS technology, the calorimeter would probably be divided into four pieces, two barrels each weighing 1425 tons and two endcaps weighing 1075 tons each. Each of these pieces would then be mated with one of the solenoid/flux return rings.

After the calorimeter is inserted into the solenoid/flux return rings, the entire solenoid/flux return/calorimeter/endcap combination is assembled on the beam line to form the final central detector. If the experimental area consists of an assembly area and a separate collision hall, the flux return/solenoid work would be done in the collision hall and the calorimeter work would be done in the assembly area. If the experimental area consists of only the collision area, the flux return/solenoid work would be done at one end and the calorimeter work would be done at the other end. Since the detector has been cut up into more or less manageable pieces (< 7500 tons), assembly of complete sections in an assembly area and subsequent movement into the collision area is not ruled out entirely if required by the schedule.

5. Tracking and Vertex Detector

Tracking and microvertex detectors have been discussed rather extensively at previous workshops [6–10]. At the Snowmass 86 Workshop [7] a rather detailed design for a central tracking system was outlined, and we refer to that report for discussions of radiation damage, rates, and occupancy. Occupancy was found to be the limiting criterion, and cell widths were chosen so that the occupancy was $\leq 10\%$ (not including bending in the magnetic field or photon conversions), although even that level may pose difficulties for pattern recognition.

5.1. Microvertex Detector

We have not worked on a new design for a microvertex detector at this Workshop, but we assumed that a large solenoid detector might include one. A microvertex detector will be useful for tagging b's and τ's, studying heavy quarks, and measuring lifetimes of new particles. A large solenoid detector is a natural place to put a microvertex detector since momentum measurement is needed for interpretation of the microvertex detector data. Low momentum tracks can acquire large impact parameters due to multiple scattering and cannot be rejected without accurate momentum measurement. We refer to the design of Snowmass 86 [6]. Such a device could be made of silicon microstrips or pixels. At present, a microvertex detector is not considered possible for luminosities greater than 10^{32} cm^{-2}s^{-1}, but improvements in radiation-hardened electronics may make operation at higher luminosities possible by the time the SSC is running.

5.2. Central Tracking

The concepts for central tracking are essentially the same as in the Snowmass 86 reports. However, we have reconsidered the requirements for momentum resolution based on the physics. We would like to measure the sign of the charge of electrons for p_T up to 0.5–1.0 TeV/c. The most severe requirements come from the measurements of W^+W^+ and W^-W^- as signs of symmetry breaking at mass scales higher than 1 TeV. The momentum resolution is given by [11]

$$\frac{\sigma_{p_T}}{p_T{}^2} = \sqrt{\frac{720}{1+5/N}} \left(\frac{\sigma_x}{0.3\,q\,B\,L^2\,\sqrt{N}} \right) \quad , \tag{1}$$

where p_T is the transverse momentum of the particle in GeV/c, q is the charge in units of the electron charge, σ_x is the spatial resolution in m, B is the magnetic field in Tesla, L is the track length in m, and N is the number of measurements, assumed to be equally spaced. We have assumed at the present time a relatively uniform distribution of wires throughout the available volume; however, it is quite possible that the final design might employ a rather different distribution.

We have assumed that the outer radius for tracking is 1.6 m, as compared with the 2.35 m used at Snowmass 86, in order to allow for all of the calorimetry to be inside the magnet coil. In calculating momentum resolution we have used 150 μm spatial resolution instead of the 200 μm used previously; this is probably reasonable since a

major contribution to spatial resolution is alignment errors and these may be less severe over a smaller radius. In addition, we have assumed a 2 T magnetic field instead of the 1.5 T used in the Snowmass 86 report. This gives a momentum resolution of $0.54p_T$ (TeV/c) for the 104 measurements assumed in our central tracker beyond a radius of 50 cm. If one uses the constraint that particles come from the interaction region the momentum resolution is improved to $0.26p_T$. The momentum resolution is improved by about the same factor for particles which come from decays of long-lived particles if a microvertex detector is used at small radius.

The tracking detector design is divided into central tracking ($|\eta| \lesssim 1.2$) and intermediate tracking ($1.2 \lesssim |\eta| < 2.5$). The central tracking chambers are assumed to have an inner radius of 40 cm. We do not expect the inner layers at radii less than 50 cm to survive at the design luminosity, but we also do not expect the SSC to begin operation at the full design luminosity. The inner layers can be removed or turned off when they are overwhelmed by the increased luminosity. Straw tube chambers are a natural candidate for a small cell design. The straws can be made small enough. They confine the sense wires to their own cell in case of breakage. They do not require a multitude of field wires resulting in large forces on the endplates. They provide mechanical support so that the chambers can be self-supporting. They provide a much better method of support than in conventional drift chambers for the long sense wires in order to achieve electrostatic stability. They can be pressurized to give better spatial resolution.

The central tracking system is assumed to be built of straw tubes of radii from 2 to 3.5 mm parallel or nearly parallel to the beam direction using a design similar to that given in Reference 12. The straws are made of aluminized polyester film (Mylar) or polycarbonate (Lexan) with wall thicknesses of about 30 μm. The straws are assumed to be at atmospheric pressure. Eight layers of straws are glued together to form superlayers, as shown in Fig. 6. Within each superlayer the layers are staggered by half the cell width in order to allow hits from out-of-time bunch crossings to be rejected and resolve left-right ambiguities as illustrated in Fig. 7. By dividing the chamber into eight-straw-thick superlayers we can obtain locally identifiable track segments with a high level of redundancy. Every other superlayer is small-angle stereo ($\sim 3°$) in order to measure the coordinate along the wire. Azimuthal cathode pad or strip readout is needed for bunch assignment since the propagation time along the wires is 16 ns for the outer layers. It is also useful to help in reducing stereo ambiguities. Cathode pad readout is included on the outer layers of the superlayers. There are 15 superlayers in all for a total of 120 measurements. The total number of cells is 122,368. The total number of radiation lengths is 8% for a particle traversing the central tracking chambers at 90°, as shown in Table IV. Thirteen superlayers are located at radii larger than 50 cm and are expected to be operable at the design luminosity. The central tracking system geometry is summarized in Table V.

The limiting factor in the momentum resolution will probably be knowledge of the relative positioning of the wires. It is difficult to see how one could use lasers to determine the alignment of straw tube chambers or chambers with many wires. One technique which could be used is mapping the wires with the help of real tracks as has been done in the

12

CLEO detector. Although spatial resolutions of about 50 μm have been achieved with straw tube chambers at 3 atmospheres absolute pressure, the problems of aligning the individual wires could well result in an effective spatial resolution much larger than 50 μm. If the alignment problems can be solved, it would be worthwhile to consider pressurizing the straws.
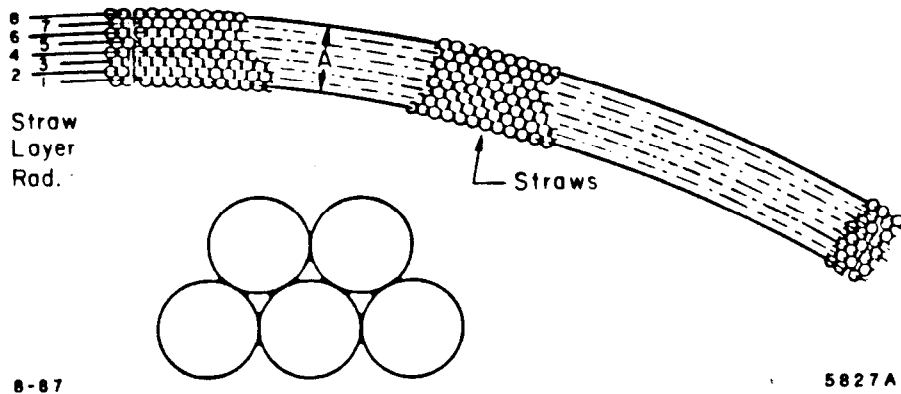

Fig. 6. Schematic drawing of a sector of a central tracking superlayer.

Fig. 7. Layers of straws in a superlayer with straws staggered by half the cell width. A single in-time track (A) will appear as a series of eight hits on the wires on alternate sides of the track. The left-right ambiguity is easily resolved locally. If two tracks are very close together (B and C), they will appear as a wide track to a single-hit readout; such a situation can be detected with a χ^2 fit. A track from an out-of-time bunch crossing is easily sorted out because the left and right drift times do not add up to the maximum drift time.
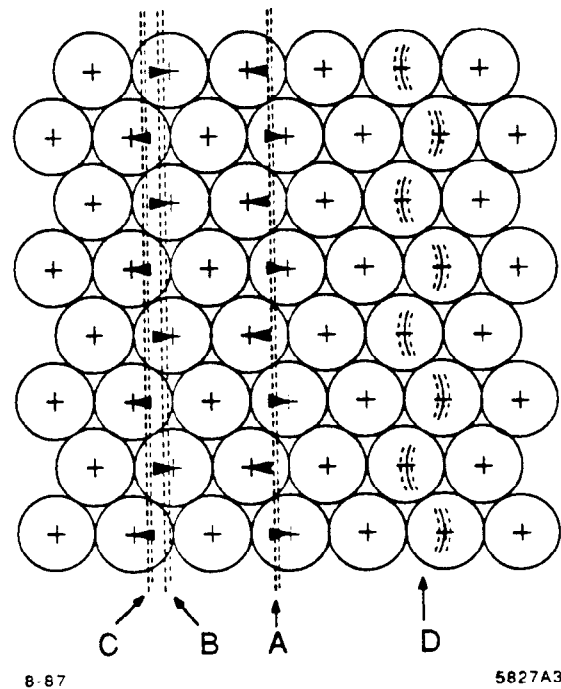

13

Table IV. Material in the Central Tracking System

Material	Thickness (cm)	Radiation Length for Material (cm)	Radiation Length (%)
Mylar	1.12	28.7	3.9
Glue	0.062	35.0	0.1
Stainless Steel Wires	0.044	1.76	2.5
Argon	50	17,800	0.3
Ethane	50	32,450	0.2
Pads on Mylar	0.15	28.7	0.5
Epoxy Foam	9.0	1,720	0.5
Total	73.5	–	8.0

Table V. Summary of Central Tracking Parameters

Superlayer Number	Inner Radius (cm)	Module Thickness (cm)	Half Length (cm)	Straw Diameter (mm)	Rapidity Range	Cell Occupancy (%)
1	40	2.7	85.2	3.92	1.50	9.7
2	48	2.7	85.2	3.92	1.34	7.3
3	56	2.7	119.0	3.92	1.50	7.0
4	64	2.7	119.0	3.92	1.38	5.6
5	72	4.1	119.0	5.89	1.28	10.4
6	80	4.2	170.0	6.04	1.50	11.6
7	88	4.2	170.0	6.17	1.41	10.3
8	96	4.3	170.0	6.28	1.34	9.3
9	104	4.4	170.0	6.38	1.27	8.4
10	112	4.5	238.5	6.47	1.50	9.5
11	120	4.5	238.5	6.55	1.44	8.7
12	128	4.6	238.5	6.61	1.38	8.0
13	136	4.6	238.5	6.68	1.33	7.4
14	144	4.6	238.5	6.73	1.28	6.8
15	152	4.7	238.5	6.78	1.23	6.3

5.3. Intermediate Tracking

In order to provide momentum measurement for $1.2 \lesssim |\eta| < 2.5$, we have added tracking in the intermediate region to take over where the central tracking ends. The intermediate tracking extends to ± 4 m along the beam line. Charged particles can be detected up to $|\eta| \leq 3.0$. The tracking chambers consist of several superchambers (at each end of the central tracking chamber), each with position measurements at several closely-spaced z values. We have considered two different designs for these chambers.

Option A. One alternative is to build planes of parallel wires between self-supporting plates consisting of 10 μm thick Mylar foils sandwiching 2 mm thick plastic foam sheets. The coordinate perpendicular to the wires is obtained in the usual fashion from the drift time. Alternate planes are offset by one half-cell to permit simple rejection of tracks from out-of-time bunch crossings. The anode wires would be every 4 mm, corresponding to a maximum drift distance of 2 mm and a sensitive time of 3 bunch crossings. The worst-hit drift cell would have an occupancy of only 2.1%. (This number should probably be doubled to account for the effects of photon conversions and for low momentum tracks which curl up in the magnetic field.)

Determination of the distance along the drift wires would be by means of 0.2 $\times$ 5 cm^2 cathode pads resistively chained together with every tenth pad being read out. The spatial resolution of such a system might be as good as 200 μm. The occupancy of a single pad cell would be less than 1.5% (3% after correction for photon conversions and curlers). The pads are arranged so that signals from two face-to-face pads can be locally correlated to depress noise and reduce the number of readout channels.

This design has 13 superchambers, each consisting of two half-moon modules with 8 anode planes each, on either side of the interaction point for a total of 104 measurements. All the wires in a superchamber are parallel to each other. The wires in each superchamber are at angles of 60° or 90° to the wires in neighboring superchambers. This option has quite low mass. The total thickness of the 13 modules is only about 7% of a radiation length for perpendicular incidence. It has the advantage of simple rejection of tracks from out-of-time bunch crossings. Local track segment finding for fairly stiff tracks should also be straightforward and might be useful for triggering purposes. On the other hand, it requires 64,000 anode wires and 250,000 cathode pad channels to be read out at each end.

Option B. A more natural geometry for a detector in a solenoidal field is one with a high degree of azimuthal symmetry. Such a geometry exists in the CDF forward radial tracking chambers [13] and in the radial chambers described by Saxon at La Thuile [9]. These chambers would have radial anode and field wires separated by stretched mylar foils with cathode pads. In order to keep the occupancy below 10%, there must be at least 800 azimuthal segments. Each superchamber consists of two sections, each with 6 anodes. The two halves are offset azimuthally by one half-cell so that, with information from 5 cm wide cathode pads, tracks from other bunch crossings can easily be rejected. There are 9 superchambers at each end of the interaction point, resulting in a total of 86,400 anode wires and 146,880 cathode pads to be read out. A track passing through the entire intermediate tracking system would have 108 measurements. Local track segment finding and momentum measurement should be straightforward. The cathode pad segmentation is also well matched to the calorimeter segmentation ($\Delta\eta = 0.03$ at the outer radius).

Local track segment finding and momentum measurement should be straightforward for either option. For example, the simple requirement that a track be radial to within 50 mrad can give one a trigger that the p_T of the track is greater than about 10 GeV/c.

The central and intermediate tracking systems are shown in Fig. 8. The momentum resolution as a function of polar angle and rapidity is shown in Fig. 9.
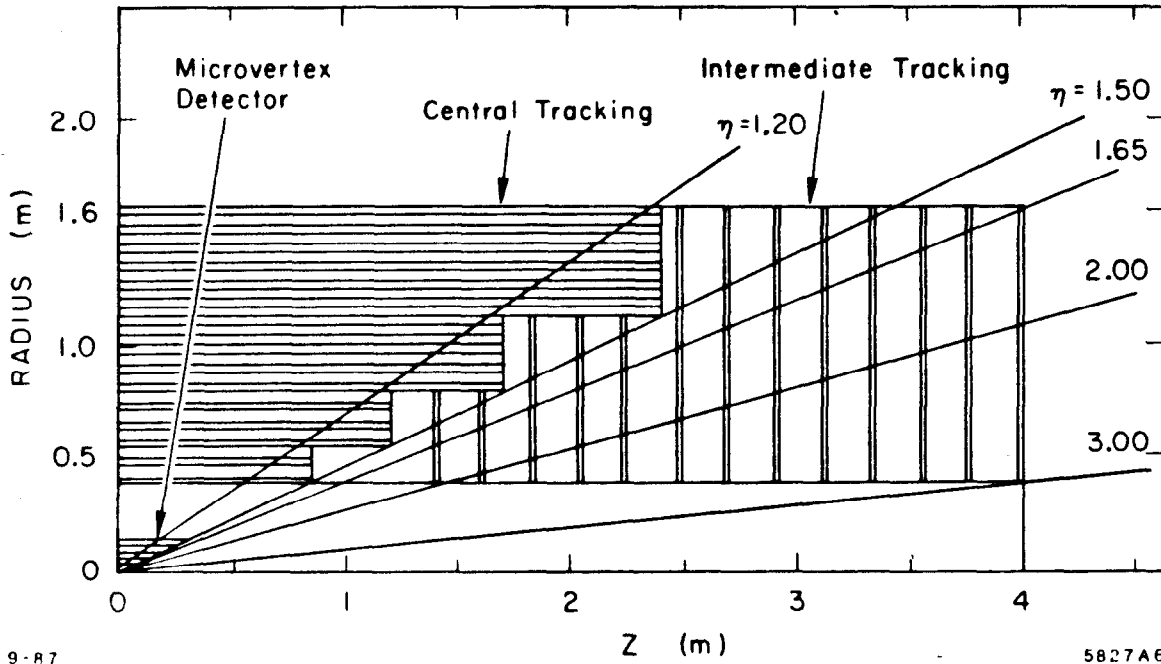

Fig. 8. Schematic view of central and intermediate tracking systems in the Large Solenoid Detector.
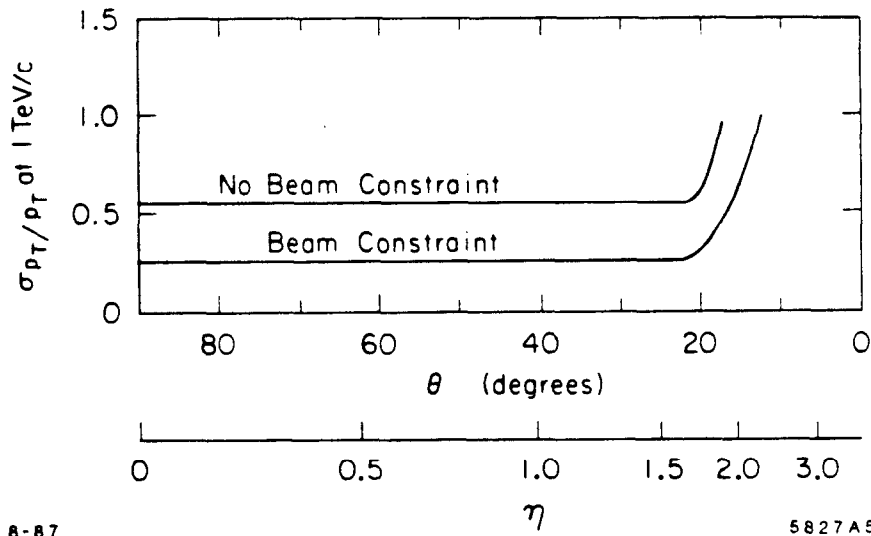

Fig. 9. Momentum resolution as a function of polar angle and rapidity in the Large Solenoid Detector for the 13 superlayers at radii > 50 cm in the central tracking system and intermediate tracking Option A.

5.4. Options at Lower and Higher Luminosities

The central and intermediate tracking described here is intended to operate at the design luminosity of 10^{33} cm^{-2}s^{-1}. At a lower luminosity of 10^{32} cm^{-2}s^{-1} the detector could include a microvertex detector and tracking at less than 50 cm radius. At a high luminosity of 10^{34} cm^{-2}s^{-1} we could turn off the tracking and still measure muon momenta outside the coil, replace the tracking system with absorber, or replace the tracking system with a new high-rate tracking system. If developments warrant, the tracking system could be replaced with a high-resolution silicon microstrip, scintillating fiber, or pixel device at a later time.

5.5. Electronics Considerations

Drift chamber tracking must be done with low gas gain ($\sim 2 \times 10^4$) in order to keep chamber lifetime and current draw at manageable levels. This means that the preamplifiers must have low noise. Straw tube chambers with diameters in the 4 to 7 mm range probably have no multihit capability because the pulse widths are approximately equal to the drift distance divided by the drift velocity. Pole-zero filters are needed to suppress the $1/t$ tail to at least allow sensitivity in the electronics to hits in the tails of hits from previous bunch crossings. Fast leading-edge timing, either from a threshold, double threshold, or constant-fraction discriminator, is needed. The time resolution should be $\leq$ 300 to 500 ps (with fast gases 1 ns corresponds to 120 μm). All of the electronics — preamplifiers, pulse shapers, discriminators, TDCs or TVCs, track processors to find track segments, and digital or analog pipelining — is expected to be located on the tracking detector in order to reduce the number of cables and processing time. The implication is that the electronics must have low power dissipation as well as radiation hardness. Electronics for cathode strips or pads is also needed.

5.6. Computer Simulation

It has not yet been demonstrated that one can solve the pattern recognition problems and find tracks in a realistic tracking system for complex SSC events with the added problems of high occupancy, hits from out-of-time bunch crossings, and more than one event in the same bunch crossing. These problems can be addressed by computer simulation of the tracking system. In addition, such a simulation can be used to study how many of the tracks can be found and to look at problems caused by photon conversions and inefficiencies due to multiple hits in the same cell. A simulation can also be used to determine the detailed design of the tracking system, including number of layers in a superlayer, how many layers of cathode strips are needed to resolve stereo ambiguities, cell width, and radial spacing of layers.

6. Calorimetry

The conceptual design of the calorimetry follows in a fairly straightforward way from the requirement that one be able to identify efficiently, and with as high a rejection of backgrounds as is possible, electrons, neutrinos (and other weakly interacting particles), quarks and gluons, and W's and Z's. These detection requirements specify the desired rapidity coverage and calorimeter thickness, transverse and longitudinal segmentation, and energy resolution. We first discuss these general properties of the calorimeter; the required values of the relevant parameters, though not optimized, are reasonably well understood. Following that we discuss which types of calorimeter construction, in particular which kind of absorber and sampling medium, are consistent with these goals.

6.1. Thickness

The overall thickness of the calorimeter is set both by the desire to obtain rather good energy resolution (of order a few per cent) for jets in the several TeV range and by the requirement of optimal missing E_T resolution. Extrapolation of existing measurements indicates that to contain 98% of the energy of a 1 TeV hadron requires a calorimeter thickness of 12 absorption lengths. Because the leading particle in a jet will have a longitudinal momentum fraction of order 0.2–0.25, energy resolutions of a few per cent may be obtained for jets of a few TeV with slightly lower thicknesses, e.g., 10–11 absorption lengths (λ). It should also be noted that measurements by different groups of the thickness required for containment of 98 or 99% of the energy of a hadron shower are not in very good agreement with one another [14]. Better measurements will be required before the thickness can be optimized. In the meantime, we assume a thickness of 10–12 λ at 90° and 13–14 λ in the forward direction.

As far as the thickness of the electromagnetic calorimeter is concerned, Monte Carlo studies [15] for the 1984 Snowmass Workshop indicated that even for an electron of 1 TeV, 26 radiation lengths will contain 98% of the energy; the thickness of the electromagnetic portion of the calorimeter was therefore taken to be 25 X_0.

6.2. Segmentation

The transverse segmentation of the electromagnetic calorimeter is determined both by the necessity for optimal identification of electrons and by the goal of detecting $W \rightarrow q\bar{q}$. Fine segmentation for electron identification is required to reject backgrounds from single hadrons and from single hadrons coincident with photons, and to enable reasonable efficiency for identifying an isolated shower in the high multiplicity environment. While it will be very difficult, if not impossible, to identify electrons arbitrarily close to a jet axis, a study [16] in the 1984 Workshop concluded that top quarks with a transverse momentum of 500 GeV/c could be identified via their semileptonic decays with an efficiency of 82% if the segmentation of the EM calorimeter was 0.02 × 0.02; the efficiency deteriorated significantly for coarser segmentations. Studies of $W \rightarrow q\bar{q}$ decays indicated that a similar segmentation was required to obtain optimal effective mass resolution if a small number of longitudinal samples were employed; good effective mass resolution for these decays is essential if one is to discriminate effectively against background from

ordinary processes [17]. However, it has also been demonstrated that good effective mass resolution for quark-antiquark decays of W's may be obtained with coarser rapidity-phi segmentation if a very large number of longitudinal readouts are employed [18]. We did not consider this option; such an approach would appear to be most relevant if one desired to build a very compact calorimeter in which case the finite shower size prevents one from obtaining as fine segmentations. The segmentation of 0.02 × 0.02 corresponds to tower sizes of order 3 cm × 3 cm in the central region, a size compatible with a determination of the shower position to an accuracy of order 2–3 mm.

The question of what segmentation is required to obtain optimal electron/pion discrimination was addressed both in the 1986 Snowmass Workshop [19] (based primarily on test results for the CDF Endplug calorimeter) and at this meeting (see Section 7 below). These studies indicate that e/π rejection ratios of 10^{-3} may be obtained with transverse segmentations of a few centimeters and with 3–4 longitudinal segments. Given these facts, and bearing in mind the desire to keep the number of electronics channels from growing too large, the EM segmentation was assumed to be of order 0.02 × 0.02 in the central region and of order 0.03 × 0.03 in the more forward regions of rapidity. In the very forward region the finite size of the electromagnetic showers renders it pointless to utilize tower sizes smaller than 1 cm × 1 cm. In this region the size of the towers in $\eta - \phi$ then increases. Each EM tower was assumed to be subdivided longitudinally into three sections; a smaller number would compromise the electron/pion discrimination given the very large range of electron energies of interest (30 GeV to 2–3 TeV) and the concomitant change in the shower length. An optimization of the segmentation, both longitudinal and transverse, for electron/pion discrimination will probably require additional studies in a test beam.

The segmentation of the hadronic calorimeter in η and ϕ was assumed to be 0.06×0.06. This corresponds to tower sizes smaller than the typical hadronic shower size (although "hadronic" showers which are largely electromagnetic will have a narrower core) and very much smaller than the typical spread of the jet. No convincing argument was made to go to finer sizes, and the consensus was that this size would probably be adequate.

In rapidity the calorimeter is assumed to cover $|\eta| < 5.5$. Numerous studies, both at this meeting and at previous workshops, have emphasized the necessity of coverage over this interval to minimize the probability of initial state gluon radiation simulating events with large missing transverse energy.

6.3. Calorimeter Composition

If the thickness and segmentation of the calorimeter seem relatively straightforward, its composition is considerably more problematic. Many combinations of absorber (uranium, lead, iron) and sampling technique (scintillator, gas, liquid argon, warm liquid, silicon) were considered. The basic criteria were that the chosen technology must support the desired segmentation, must survive the high counting rates and radiation level (with sufficiently low noise), and must provide energy resolution of a few per cent at several TeV as well as excellent missing E_T resolution.

6.3.1. Compensation

Numerous studies have indicated that in order to obtain the goals for energy resolution and sensitivity to missing E_T , the ratio of electron (or photon) response to pion response, or alternatively the ratio of the response to the EM and non-EM components of hadron showers, must be of order 1.0 ± 0.1 [20–21]. Several Monte Carlo estimates based on the measured responses to electrons and charged pions indicate that the energy resolution of calorimeters constructed with iron or copper absorber will be of order 9–11% for 400 GeV jets due to the fact that the electron/pion response is 1.4–1.6 for low energy particles [22]. In contrast, uranium and lead calorimeters are estimated to have a resolution of order 2–4% under the same conditions. In addition, the very detailed study of calorimeter performance by Wigmans [21], which includes comparison with many experimental results, enables one to predict with considerable confidence the e/h signal ratio that will be obtained with almost any combination of absorber and active medium. One of the important conclusions of this study is that while it is possible to construct a compensating calorimeter (e/h signal ratio near 1.0) with iron or copper, the very thick plates required yield a very poor energy resolution, particularly for electrons. On the other hand, it is possible to obtain compensation with excellent energy resolution with either uranium or lead. Because of the lower cost and ease of handling, lead is strongly preferred although uranium is not completely excluded. Another important conclusion of this study is that no totally active calorimeter, such as might be constructed out of liquid scintillator or BaF_2, will be compensating. We therefore focus our attention on sampling calorimeters using lead or uranium as the absorber.

Calorimeters for which excellent compensation has been demonstrated include uranium-scintillator and lead-scintillator. In addition, it is anticipated, though not yet experimentally demonstrated, that one may obtain excellent compensation with silicon or warm liquid readout [21]. Experimental results on uranium-liquid argon and lead-liquid argon indicate $e/h = 1.1$ and 1.2, respectively, but are not conclusive at the present time [22]. Theoretically, it is estimated that these combinations will not yield excellent compensation. There is some evidence that uranium-gas calorimeters can achieve compensation, although gas sampling has significant other problems as is discussed below. It should be noted that the use of uranium does not, in general, allow a denser or more compact calorimeter than the use of lead; this follows because of the different fractions of light readout material required in order to obtain compensation. For example, uranium-scintillator and lead-scintillator calorimeters each have an effective nuclear absorption length of approximately 20 cm. An exception is that silicon readout does allow a denser calorimeter to be obtained with uranium than with lead.

6.3.2. Sampling Media

We now discuss each of the possible sampling media in the light of the requirements on segmentation, speed, calibration, and stability.

Scintillator. Scintillators that are relatively radiation hard should, in principle, survive the radiation from interactions in the central region and perhaps down to angles of 10–20° [22]. For very small angles the high radiation probably requires the use of another

technique, or of a liquid scintillator which is either very radiation hard or which could be frequently exchanged. A big advantage of scintillator is the very fast response; signal collection times of tens of nanoseconds should be achievable. However, because much of the compensation relies on slow neutrons, it may be necessary to integrate for of order 100 ns in order to achieve the optimal e/π response. It has been suggested that one may be able to achieve optimal compensation at very short collection times by effectively designing the calorimeter to be overcompensated and then attenuating the compensation to the appropriate value with the short shaping time, but a systematic study of this approach has not yet been carried out.

Aside from radiation hardness, the biggest potential problems with scintillator calorimeters are the issues of calibration uniformity, stability and segmentation. Large scintillator calorimeters have been built which have been calibrated to 1% and experiments have successfully tracked the calibration over years to < 2%. No one has yet demonstrated the capability to track a large system over several years to an accuracy of 1%, although systems have been implemented which should enable one to achieve this accuracy [23].

It is difficult, if not impossible, to obtain segmentations of order 2 cm × 2 cm with the "conventional" construction which uses scintillator plates and wavelength shifters. However, considerable success has been obtained constructing lead calorimeters with scintillating fibers as the active medium. This technique should clearly allow very fine transverse segmentation. It is more difficult to achieve simultaneously the desired longitudinal segmentation in the EM calorimeter. However, schemes have been suggested which may allow one sufficient longitudinal segmentation to attain excellent electron identification, which is the primary criterion. In addition, it is possible that with very fine transverse segmentation, it may not be necessary to have such fine longitudinal response. Figure 10 presents one design for a lead-scintillating fiber calorimeter which looks very promising and is described in the contribution of Wigmans to these Proceedings. The important issues of uniformity, stability, radiation hardness, and e/π rejection ratio should be evaluated in the next couple of years.

Gas Sampling. Calorimeters which employ sampling with wire chambers or proportional tubes, which we will often refer to simply as gas calorimetry, do enable fine segmentation in both the transverse and longitudinal directions in a simple and straightforward way (by means of pad readout). In addition, such calorimeters are relatively easy to construct and reasonably inexpensive. Cracks or dead spaces in the calorimetry occupy a rather small fraction of the volume, although they certainly exist.

Disadvantages of gas calorimetry include the fact that it is less dense and it yields poorer energy resolution than liquid ionization or scintillator calorimetry. The gaps between the absorber plates are typically of order 1 cm, though at least one electromagnetic calorimeter has been constructed with gaps as small as 5 mm [24]. The energy resolution is typically 1.5–2 times worse for electromagnetic showers and 1.5 times worse for hadronic showers (for compensating calorimeters). Of greatest concern, however, are the facts that (1) it is difficult to maintain the mechanical tolerances required for the
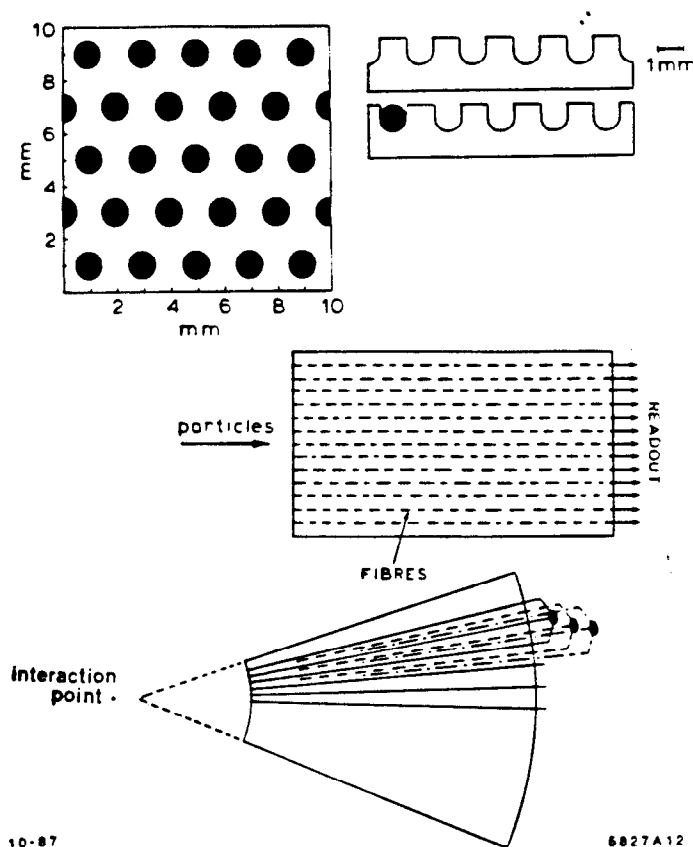
Fig. 10. Schematic design for a lead-scintillating
fiber calorimeter.

response to be uniform to 1–2% over the entire calorimeter, (2) the gain will vary with
changes in the temperature and pressure, (3) it is highly unlikely that gas calorimeters
will sustain the instantaneous rate and radiation levels in the forward direction, and (4)
the very low sampling fraction allows low energy neutrons scattering from protons to
simulate very large energy depositions (as large as 50 GeV). This latter effect, which has
proven to be a significant problem in some of the CDF gas calorimeters, could present a
very serious problem for missing E_T measurements. It is possible that this latter effect
can be strongly reduced by designing calorimeters with very low hydrogen content, and
that each of the other concerns can be overcome and dealt with in a satisfactory manner.
However, at the moment the problems seem sufficiently difficult and fundamental that
gas calorimetry does not seem a likely candidate for the primary calorimeter system.

Liquid Argon. In comparison with scintillator and gas sampling, the use of liquid
argon has a long list of advantages. The uniformity of response, both as a function of
position and as a function of time, is excellent. The goal of a systematic error of 1% should
be able to be obtained with a modest amount of effort. There is also no fundamental
problem with achieving the degree of segmentation required.

Drawbacks of the use of liquid argon include the fact that one may not be able to attain excellent compensation, the relatively slow response, and the problems of non-hermeticity due to the cryostats. As noted above, the results of experimental and theoretical investigations indicate that with lead or uranium as an absorber, such a calorimeter will yield a ratio of electron to pion response of order 1.1–1.2, the latter value corresponding to lead. While the corresponding energy resolution, typically 12–$15\%/\sqrt{E}$ for electrons and 45–$55\%/\sqrt{E}$ for hadrons may ultimately be judged to be adequate, it appears at the present time that significantly superior results may be obtained using scintillator, and possibly TMS.

Considerable study was devoted at the Snowmass 1986 Workshop to the question of noise and pileup for liquid argon calorimeters [25]. It was concluded that the charge collection times of such a calorimeter would probably be adequate for luminosities of order 10^{33} cm^{-2}s^{-1}. The estimates for noise due to electronics and pileup are summarized in Table VI. However, there is no question that a much faster sampling medium is desirable. It is quite likely that one would add a small fraction of methane to the liquid argon which would increase the drift velocity by approximately a factor of two.

Table VI. Summary of Capacitance, Equivalent Noise Charge, Equivalent Noise Energy, Risetime, Event Pileup, and Time Resolution for the Calorimeter System (from Reference 25)

Quantity	EM Slow	EM Fast	Hadronic
Pad Capacitance	0.25 nF	2.8 nF	51 nF
Stripline Capacitance	0.28 nF	0.8 nF	
Cable Capacitance	0.90 nF	1.8 nF	9 nF
Total Capacitance	1.4 nF	5.4 nF	60 nF
Risetime	325 ns	65 ns	365 ns
Measurement or Peaking Time	400 ns	100 ns	500 ns
Equivalent Noise Charge	4800 e	25000 e	30000 e
Equivalent Noise Energy	15 MeV	65 MeV	120 MeV
Uranium Noise Energy	5 MeV	7 MeV	170 MeV
Event Pileup Noise	115 MeV	120 MeV	113 MeV
Time Resolution ($E = 5$ GeV)	4 ns	2 ns	8 ns

Perhaps the most difficult problem for liquid argon calorimeters is that of attaining minimal cracks and excellent hermeticity. Of the three large liquid argon calorimeters under construction, only that for the H1 experiment at HERA approaches the uniform coverage required. The H1 calorimeter covers only approximately 60–70% of the solid angle; whether a similar approach could be utilized to cover the entire solid angle remains to be seen. Access to the detectors inside such a calorimeter is a difficult problem. One may conclude that while it may be possible to construct a hermetic liquid argon calorimeter, no one has yet demonstrated how to do it.

<u>Warm Liquids</u>. A sampling medium which potentially offers great promise, although it is not without difficulties, is TMS (or a similar warm liquid). It should allow excellent transverse and longitudinal segmentation. As for compensation, calculations have shown that the e/h signal ratio sensitively depends on the recombination properties of the liquid (Birk's constant, see contributed paper by Wigmans), which determine the calorimeter response to the densely ionizing particles that dominate the non-EM signal. An evaluation of existing experimental data suggests that Birk's constant is considerably larger than for liquid argon or plastic scintillator (0.04–0.05 g/MeV-cm^2), at least for low fields. Therefore, it may turn out to be difficult to achieve sufficient compensation with lead absorber of acceptable thickness. Of course, this remains to be experimentally verified. Difficulties with TMS, as are well known, are the flammability, very high purity required, and relatively low ionization yield at moderate field strengths. While the safety issue remains to be answered, it has been suggested that when used together with lead, rather than uranium as was originally suggested, it should be possible to design a safe system. Techniques have been demonstrated which allow sufficient purity to be obtained in very small systems; it remains to be demonstrated that this purity can be maintained over long periods of time in very large systems. While each of these issues is a significant technical challenge, there is no *a priori* reason why each may not be solved. Perhaps the ultimate determining factor will be whether a system can be designed which simultaneously achieves the desired segmentation, the required purity, and the large drift fields at a tolerable cost.

There is considerable disagreement at the present time as to whether TMS is inferior or superior to liquid argon in terms of signal-to-noise ratio. For fields on the order of 15 kV/cm and for shaping times long enough that all the ionization is collected (several hundred nanoseconds) liquid argon is clearly superior since the total collected charge/cm exceeds that for TMS by more than a factor of five. For very short shaping times (e.g., tens of nanoseconds) the situation is substantially altered since the total "useful" induced charge is proportional to the peak induced current; in this case the much higher drift velocity of TMS, approximately 15×10^5 cm/s at 15 kV/cm *vs.* 5×10^5 cm/s for liquid argon, implies that the peak induced current for TMS is nearly 60% that for liquid argon, if one assumes the free ionization yields quoted by Gonidec *et al.*[26]. Furthermore, the signal for TMS increases rapidly with electric field since the ionization yield and the drift velocity both increase as the electric field increases. Strovink, based on a study for the D0 experiment, estimates that for fields in excess of 25 kV/cm, the induced current for TMS will exceed that for liquid argon [27]. On the other hand, a comparison by Radeka [28] concludes that TMS will yield a signal-to-noise ratio about 2/3 that of liquid argon even for very short shaping times and 25 kV/cm. A significant part of this discrepancy is probably due to the fact that the ionization yields reported by Gonidec are more than 50% larger than earlier results reported by Engler and Keim [29].

Even if one assumes the larger values reported by Gonidec, it is important to note the following:

1. It may be difficult to reach shaping times significantly less than 100 ns due to the capacitance and inductance of connections in a real calorimeter.

2. The signal-to-noise ratio achievable for shaping times of several tens of nanoseconds may not be acceptable for TMS or liquid argon (thereby forcing the use of longer shaping times).

3. Addition of small amounts of methane to liquid argon increases the drift velocity, and hence the signal relative to TMS, by a factor of two.

Our conclusion is that while the obvious warm-liquid advantages of TMS give it a very high priority for R&D, the potential signal-to-noise advantages of liquid argon are such that R&D is clearly warranted to solve the cryogenic and hermeticity problems.

Silicon Sampling. The use of silicon wafers to sample the ionization energy would allow very fine segmentation, fast response, and excellent calibration and stability. It has been estimated that by including sheets of polyethylene, or similar hydrogen rich material, next to each silicon layer, silicon sampling calorimeters may attain an e/h signal response near 1.0 [21]. Whether or not silicon is sufficiently radiation hard to be used in the calorimeter has not been conclusively demonstrated. It is known that sufficient bulk damage occurs at the radiation levels at the SSC that leakage currents will be significantly increased. However, it is argued that at the very short shaping times that would be utilized, the contribution to the noise due to this leakage current would be insignificant. On the other hand, it is currently estimated that very large fluxes of neutrons will exist within the calorimeters, and the damage due to this source has not yet been thoroughly investigated.

The greatest obstacle to the use of silicon as the primary sampling medium is cost. It has been estimated that if the cost per wafer can be reduced by a factor of ten, and there is some optimism that this can be achieved, it would be possible to build compact calorimeters for use at the SSC [18]. The use of expensive high-density absorber materials (tungsten, uranium) would then be justified by the amount of money saved on silicon and on the overall size of the detector. It should be mentioned that fission neutrons from uranium absorber would increase the radiation sensitivity problems for silicon. In any case, we have concluded that for the size calorimeter envisioned for the Large Solenoid Detector, silicon is too expensive even if the goal of a times ten reduction in cost/cm^2 is achieved. It seems more likely that silicon calorimeters may be used for specialized applications.

6.3.3. Summary of Calorimeter Composition

It is quite apparent that at this point in time, one cannot choose which calorimeter type will prove to be optimal. The leading candidates together with the primary technical problems that need to be answered are:

1. Lead-scintillating fibers

   Radiation hardness

   Uniformity of response

   Long-term stability

   e/π rejection

2. Lead-TMS

Purity (including long term stability)

Measurements of Birk's constant, e/h signal ratio, and hadronic energy
resolution

Safety

High drift fields

Are materials required for finely-segmented readout (e.g., printed circuit
board techniques) consistent with required purity?

3. Lead-liquid argon

Hermeticity

Further calculations on adequacy of speed

Further measurements on e/π ratio

6.4. Size and Layout

It has often been pointed out that a barrel calorimeter which is infinitely long, and
has uniform segmentation along the beam direction, gives approximately the uniform
sampling in rapidity that is desired. Needless to say, such a geometry is not practical both
because of the overall size, and because of the acute angle between the calorimeter face and
the incident particle direction for large values of rapidity. More realistic approximations
to an ideal calorimeter have been proposed which begin with a barrel calorimeter, and
gradually make the transition to the small angle calorimeter with plates perpendicular
to the beam direction. While not explicitly indicated in the schematic diagram, we
anticipate that if a plate geometry is ultimately utilized, such as for liquid argon or TMS
sampling, a compromise between mechanical simplicity and the optimal performance
would probably result in three plate orientations: parallel to the beam in the barrel
region, perpendicular in the forward region, and at an intermediate angle in the middle
region. If lead-scintillating fiber calorimeters prove feasible, it should be possible to make
a very uniform and gradual change in the orientation as a function of rapidity.

The inner radius of the calorimeter in the present design is set by the space allowed
for the tracking; it is well matched to the calorimeter requirements, however. The inner
radius of 1.6 m at 90° allows for excellent angular information on jets, and the 4 m
distance between the face of the calorimeter at 5° and the vertex results in a minimum
tower size of 1.05 cm × 1.05 cm and in a counting rate per tower of 10^5 per second (the
latter number neglects shower spreading).

In the 1986 Snowmass Workshop, the detector design located the coil in the middle of
the calorimeter, with an internal "precision" calorimeter of 6 λ and an external "catcher"
calorimeter. Because of concern that the calorimeter performance might be significantly
compromised if the magnet coil were inserted in the middle, it was decided during this
study to explore the possibility of placing the entire calorimeter inside the magnetic field.
While the resulting magnet is quite large, such an approach appears to be quite feasible

and may greatly improve the uniformity of the calorimeter. This approach results in a more compact calorimeter, and the savings in the size of the muon system and the overall calorimeter volume in the central region may more than compensate for the larger volume of "precision" calorimetry.

7. Electron Identification

The electron identification requirements for high p_T physics at the SSC, as determined by the physics parameterization groups at this Workshop, may be summarized as follows:

1. $p_T(\text{electron}) > 10 \text{ GeV}/c$.

2. $|\eta| < 3$.

3. Hadron misidentification probability $\sim 10^{-3}$, principally for isolated particles, or jet misidentification probability $\lesssim 10^{-4}$.

Most of the high p_T-electron physics studied involves isolated electrons, with varying isolation criteria which are all coarse on the scale of the calorimeter segmentation. A notable exception is the intermediate mass Higgs particle, decaying to $b\bar{b}$. In this case, to select the b in its $b \to e\bar{\nu}_e X$ decay mode, one needs to be able to identify electrons in the b-jet, again at a $\sim 10^{-3}$ hadron rejection level. It should be noted that the requirements specified here are less severe than those stated in the Snowmass 1986 report [19,30]. In this report, we assume the goals as stated by the parametrization groups and provide evidence that an electron/pion discrimination of 10^{-3} may be obtained solely with the calorimeter and that rejections of order 3×10^{-4} may be achieved if E/p cuts are also included. An example of an "existence proof" that 10^{-3} performance can be obtained with a calorimeter is provided by the CDF beam tests of a lead-scintillator prototype shower counter [31]. We have therefore not considered in detail the use of auxiliary systems such as transition radiation devices (TRDs). However, as is discussed in greater detail at the end of this section, it is quite possible that better pion rejection will be required; in this case an auxiliary system such as TRDs should be included. We note that a nice review of the existing literature on π/e separation appears in the Report of the SSC Detector R&D Task Force [32]. We will not attempt to repeat that review here, concentrating instead on a few specific issues of central significance. We also do not discuss electron identification in the forward detector ($|\eta| > 3$).

7.1. Calorimeter Segmentation

We start by discussing the electron/pion discrimination which can be achieved with a segmented calorimeter alone, without momentum measurements, TRDs, etc. A useful test-beam study has been performed using an array of 60 lead glass bars [33]. In this study, the bars ($6.5 \times 6.5 \times 140 \text{ cm}^3$) were stacked in an array 5 across by 12 deep (total depth $\approx 24\ X_0$). Test beams of 15 to 47 GeV/c electrons and pions were measured with this array. By adding signals from various bars, the investigators were able to study the dependence of π-rejection on segmentation. With the finest segmentations, they obtained a pion rejection factor of 10^{-3}, independent of momentum in the range studied, with an electron efficiency of 90%. This result is obtained solely by the shower information in the

bars – no knowledge of the true momentum is required. We may summarize their results on the performance of various transverse and longitudinal segmentations in Table VII.

Table VII. Performance of Various Transverse and Longitudinal Segmentations

Transverse Segmentation	Longitudinal Segmentation	Pion Rejection
$5 \times 2\ X_0$	$12 \times 2\ X_0$	1×10^{-3}
$5 \times 2\ X_0$	$4 \times 6\ X_0$	1×10^{-3}
$5 \times 2\ X_0$	$4\ X_0,\ 6\ X_0,\ 6\ X_0,\ 8\ X_0$	2×10^{-3}
$5 \times 2\ X_0$	$2\ X_0,\ 6\ X_0,\ 8\ X_0,\ 8\ X_0$	2×10^{-3}
$5 \times 2\ X_0$	$3 \times 8\ X_0$	2×10^{-3}
$5 \times 2\ X_0$	$6\ X_0,\ 8\ X_0,\ 10\ X_0$	2×10^{-3}
$5 \times 2\ X_0$	$2\ X_0,\ 6\ X_0,\ 16\ X_0$	4×10^{-3}
$4\ X_0,\ 6\ X_0$	$4 \times 6\ X_0$	7×10^{-3}
$10\ X_0$	$4 \times 6\ X_0$	60×10^{-3}

We see that no advantage was obtained using longitudinal segmentations finer than 4 total segments. In the transverse direction, anything coarser than the finest available resulted in significant performance loss. Thus, this study does not reveal the ultimate limit achievable with transverse segmentation – it is possible that better than 10^{-3} rejection can be obtained with finer division, though we know of no study which demonstrates this.

It must be kept in mind when applying these results to our present problem that there are several differences between the test apparatus and the sort of calorimeter we have in mind for the SSC: (1) The SSC device will presumably have a smaller energy sampling fraction, resulting primarily in a poorer energy resolution. (2) The SSC device will have transverse segmentation in two dimensions, rather than just one. Thus, better performance may be expected, but it is unknown by what factor. The factor is unlikely to be large, because of the high correlation (approximate circular symmetry) between the two dimensions. (3) The SSC electromagnetic calorimeter will be followed by hadron calorimetry, yielding information beyond the first $\sim 25\ X_0 \sim 1\ \lambda$. (4) The test beams used covered only the lower end of the energy scale we are interested in. Since no energy dependence was observed, and since shower shape properties tend to depend logarithmically on energy, a fairly substantial extrapolation may be valid. On the other hand, exclusive charge-exchange processes tend to decrease rapidly with increasing energy, suggesting that our extrapolation might err on the conservative side. (5) A lead-glass array is principally a Čerenkov radiation device, while the calorimeter for a large solenoid SSC detector will probably be ionization-sensitive. Thus, the response to hadronic showers may be somewhat different.

Keeping the above issues in mind, we expect our calorimeter design to have a pion rejection performance (for $\sim$ 90% electron efficiency) of order 10^{-3} for isolated particles, using the shower shape information. In particular, we choose a 3-part longitudinal segmentation in the electromagnetic calorimeter of 6 X_0, 8 X_0, and 11 X_0, with the hadronic calorimeter serving as a fourth longitudinal segment. This is under the assumption that a fourth segmentation within the electromagnetic portion will not yield significant improvement because of the information provided by the hadronic section. The transverse segmentation in the electromagnetic calorimeter is nominally $\Delta\eta \times \Delta\phi = 0.02 \times 0.02 - 0.03 \times 0.03$, providing a sufficiently fine grain to separate isolated particles from jets. We may calculate the approximate segmentation dimensions in units relevant to the shower at various angles, as shown in Table VIII.

Table VIII. Segmentation Dimensions*

η	θ (degrees)	s_ϕ (cm)	$s_\phi(X_0)$	s_η (cm)
0	90	3.4	3.0	3.4
1.64	22	3.4	3.0	9.1
2.0	15.4	2.2	2.0	2.3
2.0	15.4	3.3	2.9	3.4
3.0	5.7	1.2	1.1	1.2

* For $\eta \leq 1.64$, dimensions are calculated at a nominal 170 cm radius; for $\eta > 1.64$ at a nominal 400 cm $|z|$. For the first three rows, the segmentation is $\Delta\eta \times \Delta\phi = 0.02 \times 0.02$, and for the last two rows it is 0.03×0.03. It should be noted that the distance quoted for s_η in the barrel region is the distance parallel to the beam line. In fact, the most relevant distance is the size of the tower perpendicular to the direction of the particle. Hence, for example, for $\eta = 1.64$, the effective transverse size of the tower perpendicular to the direction of the particle and in the η direction is 3.4 cm.

The dimensions in X_0 are approximate, based on 50% of the volume occupied by lead, and the active material neglected. Once the corner is turned (from barrel geometry to endcap geometry – see Fig. 1(a)) at $|\eta| \sim 1.64$, the transverse segmentation becomes finer, compared to shower dimensions. To prevent the segmentation from becoming unmanageably small, and to reduce the channel count, we propose to change from the 0.02×0.02 segmentation to 0.03×0.03 at $|\eta| = 2$. For all of the barrel region, and some of the end region, the segmentation may be coarser than the above discussions suggest would be useful. If further study verified this, we could segment the middle longitudinal segment (containing shower maximum) more finely, by a factor of 2, in the ϕ coordinate for rapidities $|\eta| \lesssim 2.0$, at a cost of $\sim$ 60k additional channels. The total number of channels in the electromagnetic calorimeter with the longitudinal and transverse segmentation as described is $\sim$ 231k, for coverage to $|\eta| = 3$. An additional $\sim$ 81k channels are needed for forward electromagnetic calorimetry.

7.2. Measurement of E/p

The ability to measure the momentum of a particle with tracking in a magnetic field allows for a comparison with the energy deposited in the calorimeter. For an electron, we expect the momentum and energy measurements to be equal within error, while for a hadron, the energy deposited in the electromagnetic calorimeter will usually be substantially less than the measured momentum. This suggests both additional hadron rejection power over the calorimeter alone, as well as a redundant check of the calorimeter information. We have investigated these issues for devices with our design resolutions.

To get an idea of the additional power obtained by adding the measurement of E/p, it is again convenient to look at the work of Reference 33. They show a graph (see Fig. 11) of the probability that a 15–47 GeV/c π^- will survive shower shape cuts, as a function of E/p. Within statistics, this probability distribution is independent of momentum over the measured range. We may use this distribution to get an estimate of the additional rejection achievable by adding a momentum measurement. For this analysis we make the simple parameterization of the distribution:

$$f(E/p) = \begin{cases} a_1 e^{b_1 E/p} & 0.0 < E/p < 0.92 \\ c & 0.92 < E/p < 0.97 \\ a_2 e^{-b_2 E/p} & 0.97 < E/p \end{cases} \quad (2)$$

(normalized to $\int_0^\infty f(x)\,dx = 1$, with $a_1 = 0.0129$, $b_1 = 6.3$, $c = 4.23$, $a_2 = 2.03 \times 10^{16}$, and $b_2 = 37.2$). The peak of the distribution is near $E/p = 1$, with a very steep fall-off above and a slower fall-off below. Thus, the shower information tends to pick hadronic showers in the electromagnetic calorimeter which contain most of the pion's initial energy, and we shouldn't expect a very large additional rejection from the added momentum information.

Use of the momentum information can be incorporated as a cut in E/p, which must be based on the resolution in E/p. For our estimates, we parameterize the momentum and electromagnetic calorimeter resolutions as:

$$\sigma_p/p = \sqrt{(a_{meas}p_T)^2 + a_{mcs}^2} \quad (3)$$

and

$$\sigma_E/E = \sqrt{(a_{samp}/\sqrt{E})^2 + a_{cal}^2 + (a_{noise}/E)^2} \quad . \quad (4)$$

Figure 12 shows the additional improvement attained by adding our E/p measurement to the shower shape rejection. The prediction above 50 GeV/c depends on the untested assumption that $f(E/p)$ remains invariant.

Reference 33 also contains a distribution for the energy deposited in the lead glass for 47 GeV/c pions before shower shape cuts. This distribution has a high peak below 1 GeV deposited energy, a broad peak near 20 GeV, and a tail extending up to the beam energy. We may apply a $\pm 2\sigma_{E/p}$ cut around $E/p = 1$ on this distribution to estimate the hadron rejection possible with a momentum-energy comparison alone (the energy
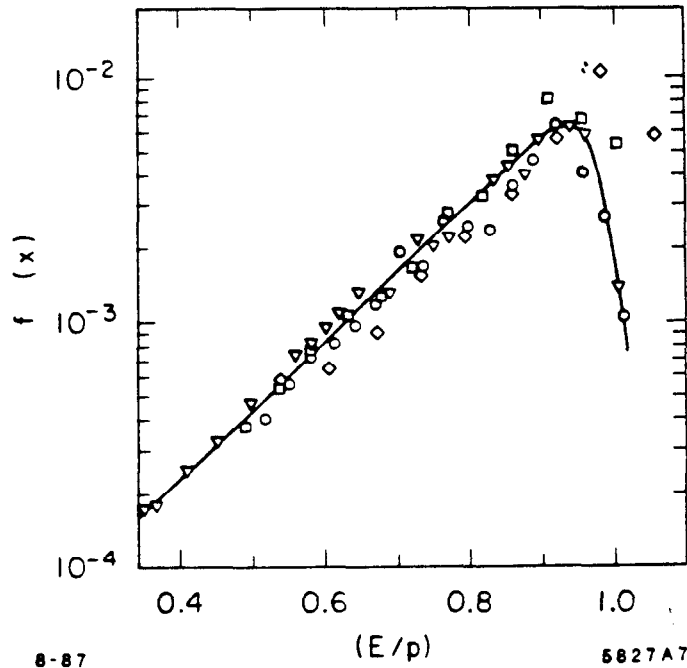
Fig. 11. Probability that a 15–47 GeV/c π^- will survive shower shape cuts, as a function of E/p (from Reference 33).

Fig. 12. Graph showing the estimated improvement factor for π rejection as a function of momentum obtained by adding a momentum measurement to the shower information from a well-segmented calorimeter which achieves 10^{-3} rejection before the momentum information. A $\pm 2\sigma$ cut in E/p is used. The energy and momentum resolutions (see text) are calculated with $a_{mcs} = 0.01$, $a_{cal} = 0.01$, and $a_{noise} = 0.5$ GeV. The solid curves are with $a_{meas} = 0.00026\,(\text{GeV}/c)^{-1}$, as appropriate for a beam-constrained momentum measurement, and the dashed curves are for $a_{meas} = 0.00054\,(\text{GeV}/c)^{-1}$, corresponding to no beam-constraint. For each pair of curves, the top one is with $a_{samp} = 0.10\,\text{GeV}^{\frac{1}{2}}$ and the bottom one is with $a_{samp} = 0.15\,\text{GeV}^{\frac{1}{2}}$.
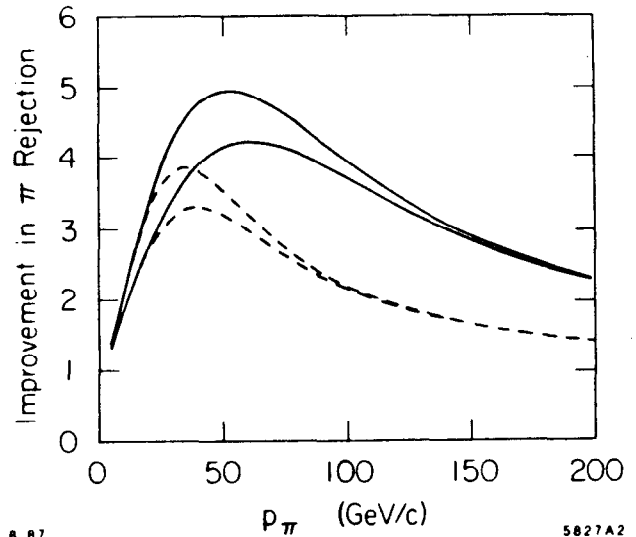
resolution of the lead-glass array is good enough to be neglected in this estimate). The result is a rejection of ~ 2–3×10^{-3}, with an additional uncertainty of perhaps 50% from residual electron contamination in the pion beam.

We conclude this discussion with the following observations: Using the calorimeter information alone, a pion rejection of $\sim 10^{-3}$ is possible, and using E/p alone a rejection of a few $\times 10^{-3}$, at least for 50 GeV/c pions. Adding the E/p information to the shower rejection improves the rejection power by factors of a few. There is substantial correlation between the two methods, so they are primarily redundant rather than independent methods. Having both approaches means that they can be used as cross checks on each other. Furthermore, one method, E/p, is most powerful for $|\eta| \lesssim 1.6$, where the momentum resolution is best, and the other method is most powerful for $1.6 \lesssim |\eta| \lesssim 3.0$, where the transverse segmentation is best. Thus, we expect to be able to meet the desired specification for all $|\eta| \lesssim 3.0$ by using the two methods. While we have concentrated our discussion on truly isolated particles, it is worth noting that the E/p information is extremely valuable in rejecting situations with photons overlapping $\pi^{\pm}$ tracks [19]. It also should be noted that tracking in a magnetic field enhances our ability to reject backgrounds from Dalitz pairs and converted photons. The separation, s, of the e^{+} and e^{-} from the symmetric conversion of a photon of energy E_{γ}, after traversing 1 meter in radial distance from the conversion point is given by $s \approx [1.2/E_{\gamma}(\text{TeV})]$ mm, assuming a 2 Tesla field. Thus, the separation is readily detected up to quite high energies. It should finally be stressed that we have based our estimates heavily on the detailed information available at ~ 50 GeV/c – studies with realistic and flexible prototypes at higher test beam energies will be a crucial step in any rational design process for an SSC calorimeter.

7.3. Transition and Synchrotron Radiation Devices

Given the preceding discussion, and the specifications put forward by the physics parameterization subgroups, it can be concluded that an appropriately segmented calorimeter, plus some momentum measurement capability, will be sufficient to do the physics. However, as noted above, we have varying degrees of discomfort on this matter for the following reasons: First, there is some concern that the conclusions of the parameterization groups may understate the requirements. Perhaps the background studies have so far been insufficiently comprehensive or realistic. This concern is fueled partly by the more stringent requirement (10^{-4} or even 10^{-5} hadron misidentification) stated at the Snowmass 86 Workshop [19,30], although those numbers do not appear to have been the result of an exhaustive study. Second, even if the parameterization studies are accurate, there may be other physics not considered. A more conservative approach to the question of how well we might ultimately wish to do at hadron rejection is to ask what rejection is required to reduce the hadron background below the level of real "prompt" electrons. Thus, for isolated particles, we first ask how often an isolated hadron occurs in the background processes (as a function of p_T), and then what further rejection is needed to get the level below the rate of electrons from b, t and W decays. A careful investigation along these lines has not been completed, but is essential in order to understand what level of hadron rejection is optimal. Third, the calorimetric methods of electron identification are

difficult when in the environment of a jet. Fortunately, this is not the typical situation of interest, but one example does exist – the decay of an intermediate mass Higgs to $b\bar{b}$. In this case, the b-jet has a fairly small p_T, so it is not hopeless; but it is marginal whether the required performance can be achieved without additional devices. Fourth, even if the 10^{-3} rejection level is adequate at $10^{33}\,\mathrm{cm}^{-2}\mathrm{s}^{-1}$, a higher-luminosity upgrade would probably be looking for rarer signals, requiring proportionately better rejection.

Because of these concerns, we feel it is imperative to keep the option available of installing additional devices for electron identification. This need for flexibility is a major argument for not shrinking the size of the central cavity any further. For example, a TRD design from Snowmass 86 requires about 60 cm in radius for four TRDs. Currently, the candidate devices with the most promise are TRDs and SRDs. Both types of device are being used in existing experiments. These possibilities, along with the difficulties requiring further study for application at the SSC, are described in References 19, 30, and 32. There is also a recent general review of TRDs by Dolgoshein [34].

An interesting idea for using TRDs in a high-luminosity environment is to turn the hardware threshold up above $\sim 8\,\mathrm{keV}$ (we imagine the Snowmass 86 design, consisting of TRDs with 100 layers of 40 micron polypropylene foil followed by a 50-50% Xe-C_2H_6 X-ray wire chamber detector). Then the many uninteresting pions below ~ 300 GeV/c are effectively invisible in this device, electron identification below this momentum is available, and the TRDs may be used for tracking both pions and electrons above ~ 300 GeV/c.

8. Muon Identification and Momentum Measurement

The goal of the muon detector system in the Large Solenoid Detector is to identify and measure the vector momenta of muons between about 10 GeV/c and 2 TeV/c and over a rapidity range of $\pm$ 5 units. The system chosen in this detector takes strong advantage of the fully integrated functional nature of the Large Solenoid Detector, integrating the muon momentum measurements with the central tracking detector, the large solenoid magnetic flux return yoke and the hadron calorimetry (all of which is located within the solenoid coil). Muons at small angles (less than about 30°) are measured by means of conventional magnetized iron toroids placed around the beam pipe and shaped to permit muon momentum measurements at all angles down to 0.8°. The relationship of the detector elements is shown in Fig. 1(a). The particular subsystem aspects of the muon detector are now discussed in some detail.

8.1. Momentum Measurement of Large-Angle Muons

Large-angle ($\theta > 30°$) muons leaving the interaction region are picked up by the central and intermediate tracking systems, allowing a partial orbit determination to be made. They then pass through the calorimeter where they undergo multiple scattering in the absorber material. As they exit the calorimeter and after they pass through the magnet coil, their positions and slopes are measured by modules of drift tubes located between the solenoid coil in its cryostat and the iron flux return yoke of the magnet. It is assumed that the spatial location precision of points along the orbit in the bending

direction can be held within a combined statistical and systematic error of 50 μm at this position together with an angular measurement lever arm of 50 cm. It is further assumed that the longitudinal position parallel to the beam can be determined within an error of a few centimeters using current division or induced cathode charge measurements. These achievable error assumptions relate directly to the momentum resolution capability of the muon system (for high momenta especially).
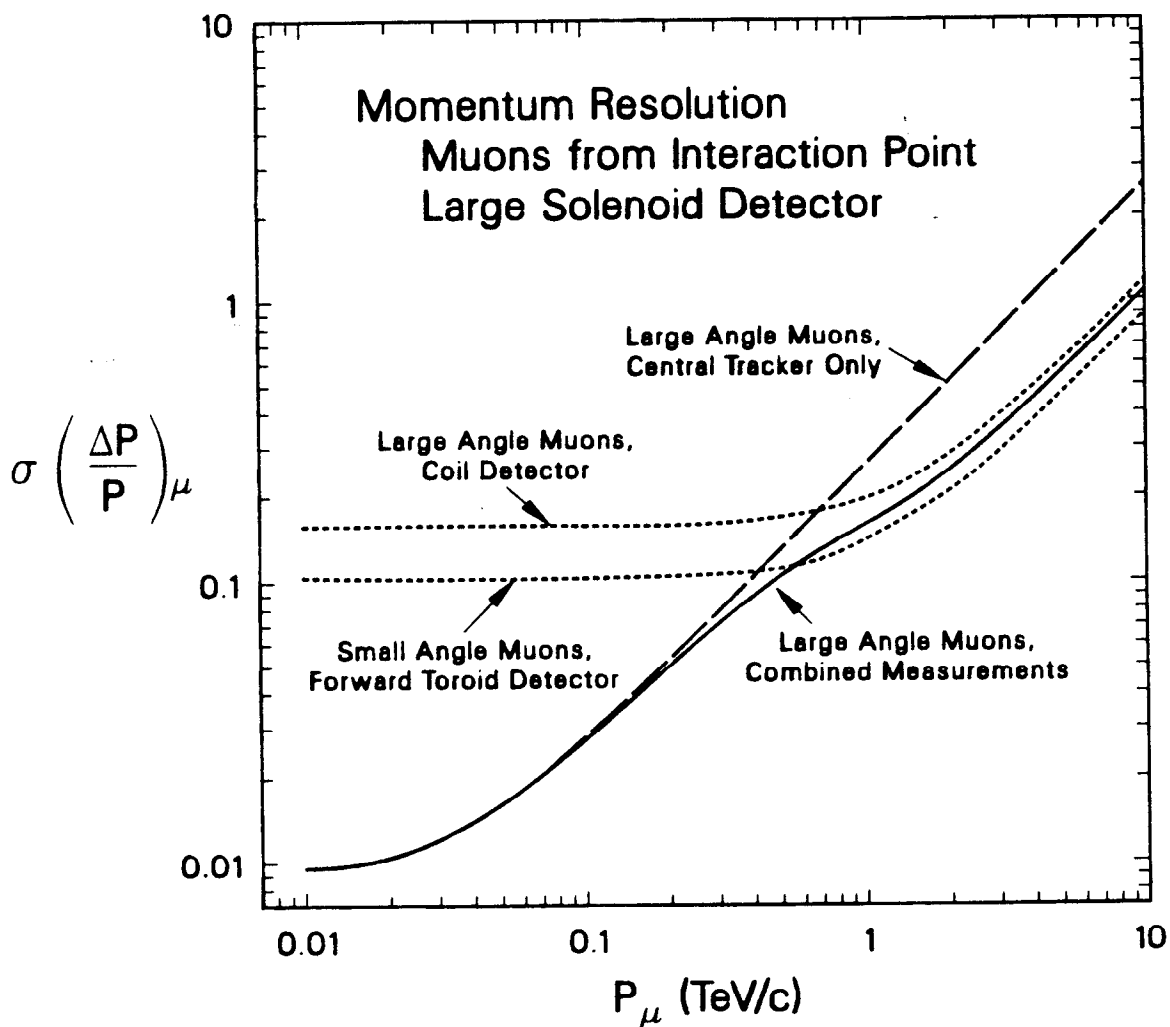
For large-angle muon momenta *below* about 500 GeV/c, a classic orbit sagitta measurement can be accomplished *entirely within* the central tracking devices; the muon momentum, therefore, is well measured using data only from these detectors. The muon *particle identification function* is, of course, established in all cases by its subsequent penetration through the calorimeter and magnetized iron material outside the tracker. For muon momenta *above* 500 GeV/c, the added magnet track length gained by measuring the muon's magnetic trajectory *through the calorimeter* (with the drift tube modules) allows a very significant gain to be made in $B\,L^2$, hence in muon momentum resolution. This gain in resolution is made because the spatial resolution in sagitta measurement takes over from multiple scattering as the dominant source of error as muon momenta increase above this value.

The large-angle muons then pass through the magnetized iron return yoke where a third, largely independent, momentum measurement can be obtained by deflection in the yoke iron. The muon positions are measured once more on exiting the yoke and the deflection angle determined to an accuracy of 0.14 mrad. This angular precision assumes, as before, that the outside muon drift tube modules can be maintained in space with a statistical and systematic location error not exceeding 50 μm and that a 0.5 meter lever arm for measuring the exit angle is available. These assumptions present severe technical challenges and appropriate technology will need to be identified and developed to insure that these tolerances can be met.

Under the conditions noted in the paragraphs above, the muon momentum is measured at large angles with the fractional precision shown in Fig. 13. Even if the final exit angle from the magnetized iron yoke is not measured, the momentum precision is not degraded for most conditions (it is largely dependent on the measured angle of deflection in the central solenoid field); the valuable particle identification constraint of having a third, backup momentum determination is lost, however.

The momentum resolution graph for large-angle muons (displayed in Fig. 13) is dominated by two sources of measurement uncertainty: multiple Coulomb scattering and spatial resolution. Spatial resolution in the central tracking detector dominates the overall momentum resolution for large-angle muon momenta below about 400 GeV/c and a combination of both error sources contributes significantly in the full coil measurement path for momenta above this value. Shown in Fig. 13 is a significant gain in resolution realized by combining the two measurement methods available for large-angle muons. Of special interest is the ability of the adopted muon system to generate an electric charge sign determination for muon momenta up to about 2 TeV/c. Since the momentum measurement errors are Gaussian for the *reciprocal* of the momentum, a second graph is
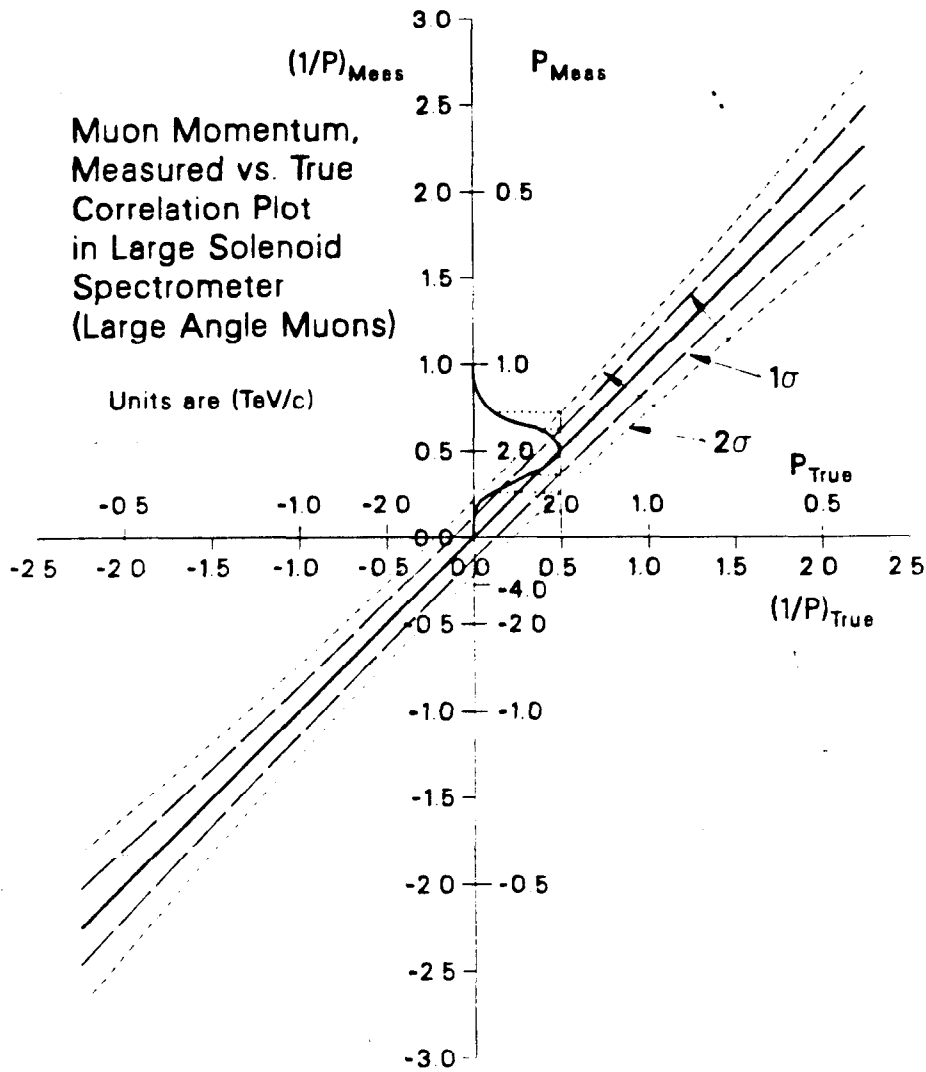
presented which shows the reciprocal momentum measurement error (Fig. 14). This graph allows an easier assessment of the probability of making large fractional momentum errors, or of errors in determining the electric charge sign for very high momentum muons. In the example shown, it is seen that a 2 TeV/c muon has a 2 standard deviation probability for misdetermination of the electric charge sign. To assess the magnitude of measurement errors from multiple Coulomb scattering, the calorimeter was assumed to have lead absorber plates distributed uniformly over the radial zone from 1.6 to 3.6 m in the central region, and to have a total thickness of 1900 gm/cm^2 of lead (300 X_0, 10 λ). As the angle of incidence decreases from 90°, the effective absorber thickness will increase, as will the amount of multiple scattering. There will also be a decrease in momentum measurement precision for muons below an angle of about 30° as the full turning angle in the solenoid is decreased.

Momentum Resolution
Muons from Interaction Point
Large Solenoid Detector

Large Angle Muons,
Central Tracker Only

Large Angle Muons,
Coil Detector

Small Angle Muons,
Forward Toroid Detector

Large Angle Muons,
Combined Measurements

$\sigma \left(\dfrac{\Delta P}{P} \right)_\mu$

P_μ (TeV/c)

5827A13
XCG 878-11359 A

10-87

Fig. 13. Momentum resolution for measurement of large-angle and forward-going muons in the Large Solenoid Detector.

$(1/P)_{Meas}$ P_{Meas}

3.0

Muon Momentum,
Measured vs. True
Correlation Plot
in Large Solenoid
Spectrometer
(Large Angle Muons)

2.5
2.0 — 0.5
1.5
1.0 — 1.0

Units are (TeV/c)

0.5 — 2.0

1σ

2σ P_{True}

-0.5   -1.0   -2.0   2.0   1.0   0.5

-2.5   -2.0   -1.5   -1.0   -0.5   0.0   0.5   1.0   1.5   2.0   2.5

0.0

-4.0

0.5 — -2.0

$(1/P)_{True}$

-1.0 — -1.0

-1.5

-2.0 — -0.5

-2.5

-3.0

5827A14
XCG 878-11360 A

10-87

Fig. 14. Gaussian error contours for reciprocal muon momentum measurements in the Large Solenoid Detector.

8.2. Momentum Measurement of Small-Angle Muons

In the small-angle forward regime, muons are measured by deflection through magnetized iron toroids (see Fig. 1(a)). To suppress loss of measuring ability through the track-obscuring effects of soft electromagnetic showers in the toroids, redundant samples are taken of the muon position at two points within the toroids and a final angle is measured behind them. The entering muon angle is determined by the forward tracking system.

The muon momentum resolution for small-angle muons is shown in Fig. 13 for comparison with the resolution for large-angle muons. The small-angle detector elements are multi-layer muon proportional tube modules interspersed with magnetized iron toroids.

36

A module is assumed to generate a space point with 50 μm resolution in the bending direction. The resolution at small angles is seen to be comparable to or better than that at large angles for momenta above 500 GeV/c. Below this momentum, the solenoid field topology is intrinsically limited in its analyzing power for small-angle muons (less rotation angle in the field) and the observed resolution deteriorates to its multiple-scattering dominated asymptote for the smallest-angle muons (trajectories essentially parallel to the central tracker magnetic field direction).

Rate effects for SSC luminosities and their influence on detection of small-angle muons, as well as the problem of muon-generated soft showers and large (non-stochastic) fractional energy losses in thick absorbers were investigated and described in the Snowmass 86 Proceedings [35] and will not be covered again here. These problems were not felt to be severe for most experimental purposes.

9. Trigger and Data Acquisition
9.1. Trigger

Detectors at the SSC will require a high level of sophistication in the trigger. Triggering on many physics processes in parallel with simple loose triggers will lead to a very high trigger rate. Moreover, in most cases, the interesting, rare physics processes do not stand out distinctly from the QCD backgrounds. It will be necessary to have a rather sophisticated on-line trigger in order to trigger on the interesting processes at a reasonable rate. Fortunately, the signatures of all physics processes consist of the same fundamental ingredients, electrons and muons, usually isolated, jets, and missing E_T, thereby providing a small number of basic trigger ingredients from which parallel triggers are built.

The general architecture of a multi-tiered trigger system for a large solenoid detector has been discussed at previous workshops, particularly at the Workshop on Triggering, Data Acquisition, and Computing for High Energy/High Luminosity Hadron–Hadron Colliders [36] at Fermilab in November 1985. The multi-tiered scheme is dictated by limitations to the ability to buffer and transfer large blocks of detector data until a final trigger decision is complete. Each tier rejects a large fraction of the event candidates received from the previous tier, thereby affording the next tier more time to make a more sophisticated decision to reject further events. The first tier, or Level 1, is usually considered to make the most rapid decision possible, using analog sums of calorimeter data and at least some clustering to obtain a rejection of 10^3–10^4 in about 1 μs. Level 2 is then allowed about 10 μs to reject an additional factor of 10^2 using more detailed considerations, such as the distribution and clustering of energy and the association of charged tracks with electromagnetic energy. Finally, Level 3, which is itself multi-tiered, has available for the first time all the data from all parts of the detector. It then uses a large farm of microprocessors to reject an additional factor of about 10^2, reducing the final event rate to 1–10 Hz. Table IX, borrowed from the report of the Physics Signatures Working Group [37] at the Fermilab Triggering Workshop, illustrates how one path in a parallel trigger might select Higgs events of the sort:

$$H \to W + W \to e + \nu + jet + jet \quad .$$

Table IX. Summary of Trigger Strategy and ISAJET Results for $H \to W^+ + W^-$. Note that the rejection factors apply to individual cuts while the efficiencies are cumulative.

Trigger Selections	Rejection Factor	Remaining Cross Section (nb)	$H \to WW$ Efficiency
First Level: (a) Select electron candidate as calorimeter cell with $E_T > 25$ GeV and with at least 80% of the energy electromagnetic	700	3×10^4	0.86
Require $p_T^{miss} > 40$ GeV/c for the event	4	7500	0.43
Second Level: Require the electron candidate to be isolated, with a surrounding region of ± 5 calorimeter cells in both η and ϕ containing less than 20% of the E_T of the electron candidate cell	1.3	5700	0.37
(b) Make a jet requirement of either 1 jet having $E_T > 80$ GeV or 2 jets each having $E_T > 40$ GeV	20	290	0.32
Third Level: Require that tracking show a charged particle with $p_T > 10$ GeV/c pointing to the candidate electron calorimeter cell	255	1.1	0.32

Note that the "Third Level" trigger selection of the previous example required a charged track with $p_T > 10$ GeV/c and pointing to the candidate electron calorimeter cell. It is therefore very important that one have some minimum cut on charged track momentum in the trigger; this could be accomplished either by reconstructing the momenta of stiff tracks or by use of TRD information. One method for determining the p_T of a charged track associated with a cluster of electromagnetic energy in the calorimeter is to measure the angle of the track in the outer superlayer (group of 8 layers) of the central tracking system. For moderate momenta, sufficient angular resolution exists, even without realizing at the trigger level the full spatial resolution of the drift chamber. Thus, the magnetic field provides an additional tool at the trigger level to reducing backgrounds to electron candidates.

The above example of Higgs decay into W-pairs is but one example of many interesting physics processes upon which to trigger. It appears to be a manageable example as described by the Fermilab Triggering Workshop; however, it is a relatively easy example. For each other physics process of interest a set of analysis cuts must be defined in order that a set of realistic on-line trigger cuts can be chosen. Then a conceptual design for trigger algorithms, including appropriate hardware, can be developed for representative detector topologies. At that stage, two crucial issues can be addressed. First, since the

time required for trigger decisions will depend on detector topology, are there important implications for the detector topology? For instance, does matching charged tracks to electromagnetic showers prefer a particular geometry of tracking chambers, or is there an appropriate segmentation for a transition radiation detector to match it to the calorimeter? Second, how sharp must cuts be at the trigger level; for instance, what p_T resolution is needed at the trigger level to efficiently trigger on electrons from $W \rightarrow e\nu$ without excessive trigger rates from background? This consideration will impact the uniformity of response necessary from detectors and electronics and will determine what calibration corrections will be needed at the trigger level. Since details of the trigger affect the details of detector design in such ways, the trigger must be realistically included in simulations of detector designs. The difficult triggering environment at the SSC demands that the trigger be considered as part of the interplay of physics goals and detector design.

9.2. Data Acquisition

The general aspects of data acquisition for a large solenoid detector were described by the report of the Data Filtering/Acquisition Group at the November 1985 Workshop on Triggering, Data Acquisition, and Computing for High Energy/High Luminosity Hadron-Hadron Colliders at Fermilab [38]. The data acquisition electronics includes detector-mounted custom VLSI circuits to amplify, shape, and sample the detector signals and to buffer the samples during Level 1 and Level 2 trigger decisions. During the Level 1 decision, samples from all beam crossings must be buffered, and during the Level 2 decision, samples from all Level 1 triggers must be buffered. An example of this "front-end" electronics was also presented at the Fermilab Workshop [39]. More detailed examples of electronics for drift-time measurement and calorimetric measurement were described in the report of the Triggering and Electronics Group at the Snowmass 1986 Summer Study [40]. These workshops highlighted the concerns of power dissipation and radiation hardness and the need for VLSI R&D for both the amplifying/shaping and the sampling/buffering functions. The front-end electronics must also preprocess and sparse scan the data for each Level 2 trigger in order to limit the required bandwidth at the output of the front-end electronics.

Trigger requirements will impact the design of the front-end electronics; however, the implications have not yet been explored. Note that the quantity of data in the front-end buffers is tremendous and the portion of this data which can be used in the trigger may be limited by the bandwidth of the connections and busses linking the front-end electronics to the trigger processors. Locating a large part of the trigger electronics at the front-end electronics and segmenting the trigger electronics in a geographical way will ease this bandwidth issue and at the same time provide parallelism in the trigger processing which is needed for prompt trigger decisions. Examples of local and geographic trigger processing include local shower clustering and local track segment finding.

Conceptually, all sparse-scanned data from Level 2 triggers is transferred via event builders to the Level 3 trigger processors, which are a farm of general-purpose microprocessors. This portion of the data acquisition system perhaps looks more conventional than the front-end electronics; however, the necessary bandwidths and processing power far

exceed systems currently being implemented. We should be encouraged by the experience now being gained, and soon to be gained, with microprocessor farms in several existing detectors. Nonetheless, new hardware and, perhaps more importantly, new software tools will be needed to manage this data and processing.

The task of producing particle four-vectors, which has traditionally been performed off-line, may be efficiently performed on-line at the SSC. The basic tasks of reconstructing energy clusters and charged tracks and of associating particle identification attributes will be performed to a large extent in the trigger and the Level 3 processors. Retaining this information, even if further refinement in on-line algorithms is necessary, will lead to economies in computing. Furthermore, reducing the raw data to reconstructed tracks and parameters on-line will lead to economies in data handling and bandwidth, which if used judiciously can increase the acceptance of interesting physics events and processes.

In summary, the detailed architecture of the data acquisition system is yet to be developed. It will to a large extent be determined by considerations of power and of bandwidth. Economies in how much data is buffered, transferred, and processed will alleviate these concerns. Thus, the details of the distribution of processing within the architecture sketched above will be significant.

10. Research and Development Requirements

A considerable amount of research and development will be required before a large solenoid detector for the SSC can be designed and built. The time needed for R&D, design, and construction for this type of detector is probably commensurate with the time scale for building the SSC itself since the detector concepts are rather well understood. The research and development requirements for the various detector components are described in the following sections.

10.1. Solenoid Magnet

The main work needed here is not so much R&D since we have chosen an existing superconductor but an honest engineering conceptual design to determine the feasibility of producing the proposed solenoid and flux return and the cost of such an undertaking.

10.2. Tracking and Vertex Detection

There are many areas in which research and development are required for tracking in a large solenoid detector. The high-rate and high-radiation environment provides considerable challenges.

Vertex Detectors and High-Resolution Tracking Devices. While vertex detectors were not discussed in detail by this group, we assumed that a large solenoid detector would include one. For completeness, we will mention some of the R&D required, although more detail can be found in other reports in these Proceedings. The main problem for silicon microstrip and pixel detectors is radiation sensitivity of the detector itself and the electronics, particularly since they need to be located close to the beam line. In addition, the electronics needs to have low power dissipation. The main areas for R&D

for scintillating fibers are short attenuation length in small-diameter glass fibers and long fluorescence decay times and readout times.

Central and Intermediate Tracking. Some of the major requirements for research and development for central and intermediate tracking for a large solenoid detector are listed here.

1. There are many mechanical and electrical problems involved in building a central tracking system out of long straw-tube chambers. What is the minimum wall thickness required? How can long straws be handled, held straight, and positioned? How well can the wires be positioned? How can the wires be supported for electrostatic stability? Can a chamber be built with stereo straws? How can cathode pads be implemented? Are pressurized straws a realistic possibility? Feasibility studies are needed.

2. Much more work is needed even at the conceptual design stage for intermediate tracking. The two options described here, planes of parallel wires and radial tracking chambers, are possibilities, but a more attractive solution may be found after more work. The two options described require a large number of cathode pads for reading out the coordinate along the wire. Their pattern recognition capabilities need study. Either option also involves mechanical design problems.

3. "Fast" drift chamber gases, such as mixtures of CF_4, could be very useful in reducing the occupancy for a fixed cell size or reducing the number of cells by allowing a larger cell for a fixed occupancy. More research is needed on these gases to determine their radiation resistance, spatial resolution, double-hit resolution, and operation characteristics in moderate magnetic fields.

4. Efforts are needed in understanding how to align or measure the position of the wires. Systematic errors in wire position will probably be the limiting factor in the momentum resolution obtained with any wire chamber system.

5. At this time it is not clear whether we will need to record multiple hits for each wire or digitize the pulses. Straw-tube chambers probably do not have multi-hit capability. R&D is needed in this area.

6. Computer simulation is needed to study pattern recognition in the high-rate SSC environment. For central and intermediate tracking the dominant constraint is the combination of cell occupancy and double-hit resolution. It is crucial to determine what tracks can actually be found for SSC events given the high multiplicity and density of tracks and the added hits from out-of-time bunch crossings. Pattern recognition studies are also needed for high-resolution tracking devices such as silicon microstrip and pixel devices. Computer simulation can then be used to determine suitable mixes of pixel devices, silicon strip devices, high-precision drift chambers, and large straw tube or drift chamber systems for a large solenoid detector. Finally, computer simulation can be used to help determine the detailed cell and tracking system designs.

41

10.3. Calorimetry

Fundamental questions must be answered by research and development and by experience with running or proposed detectors before a choice can be made from among the three most attractive options for calorimetry in a large solenoid detector. The major areas for R&D are listed below.

Lead/Scintillating Fibers. The possible problems for this type of calorimeter are radiation hardness, calibration uniformity and stability of response, long-term stability, and sufficient longitudinal segmentation to obtain e/π rejection of at least 10^{-3}.

Lead/TMS. Operational experience with warm liquid calorimeters is needed to determine whether the conditions for safety and purity can be met. High drift fields are needed to increase the induced signal current to at least the level of liquid argon. Birk's constant and the e/h signal ratio need to be determined experimentally; it may turn out to be difficult to achieve sufficient compensation. Hadronic energy resolution should be measured. Although there are important technical problems to be solved, warm liquid calorimeters may ultimately prove to be better able to meet the hermeticity requirement for calorimeters at the SSC.

Lead/Liquid Argon. Liquid argon calorimeters have been used quite successfully in the past; however, the requirements for calorimetry for a large solenoid detector at the SSC may be difficult to meet with liquid argon. Hermeticity is probably the hardest problem to solve. The cryostat must be designed so that cracks are minimized. Compensation is also a problem which needs experimental investigation. Further calculations are needed to determine whether the charge collection time is adequate for the SSC.

Beam Tests. For any calorimeter design beam tests will be needed to measure the e/π ratio and hadronic and electromagnetic energy resolution.

10.4. Electron Identification

In addition to R&D on calorimetry, outlined in the previous section, more development of TRD technology relevant to the high energies at the SSC is needed to prove the feasibility of some of the ideas that have been proposed, in particular to push the energy range up to 300 GeV or more. Likewise, studies of realistic synchrotron radiation devices would be useful to determine feasibility in the SSC environment.

10.5. Muon Identification and Momentum Measurement

Specific areas for R&D for muon detection include spatial alignment of the tracking detectors and stability as a function of time and temperature. In addition, integration of the muon detector wire geometry into the processing required for low-level triggering should be studied. R&D is also needed concerning the effects of interactions of high-energy muons with material on muon identification and triggering.

10.6. Electronics

The high interaction rates at the SSC lead to an overall data acquisition scheme (see Section 9.2) based upon highly integrated and sophisticated systems of front-end electronics mounted on the detector. Development and construction times for electronics for present detectors already frequently exceed times for mechanical systems. Moreover, the front-end electronics designs will be integrated into the mechanical designs and the data acquisition system. These front-end circuits will be the most challenging R&D problem in electronics. Timely R&D of front-end electronics is essential to SSC physics.

Some areas for R&D for front-end electronics were listed in the report of the Snowmass 86 Triggering and Electronics Group [40]. In some respects, custom VLSIs developed for current experiments, such as analog memory devices for SLD, microplex readout of silicon strips for Mark II and DELPHI, and pipelined readout of calorimeters for ZEUS, serve as models for SSC electronics. However, these circuits are in general not adequate for the SSC with respect to scale of integration, readout times, power consumption, radiation hardness, and system design.

R&D for front-end electronics for a large solenoid detector should take two directions. The first direction should be generic studies. For instance, different integrated circuit technologies should be examined for their appropriateness to the SSC. In addition, relative advantages of various pipeline structures should be studied, such as CCDs vs. switched capacitors or digital vs. analog, with respect to speed, charge resolution, power and calibration aspects. Techniques for improving radiation hardness should also be investigated. The second direction should be the development of front-end electronics circuits for specific detector components. Prototypical circuits for drift-time and charge measurement should be built in order to demonstrate the principle of the SSC data acquisition scheme and to gain experience with the techniques. The circuits could be tested in an actual experimental environment. The detailed design of these circuits, however, depends on the detailed design of the detector, including signal risetime, detector capacitance, detector and cabling impedance, packaging, etc., and on the details of the overall data acquisition system. Circuits for third coordinate readout in tracking chambers – delay lines, charge division, and cathode pads – must be developed. In addition, circuits for simultaneous measurement of time and pulse height will be developed. Front-end circuits for finely-segmented silicon devices, much different from existing multiplexed designs, will be needed. In light of the long lead times involved in developing and producing front-end circuits and their dependence on system concerns, R&D on some of the details of the overall data acquisition system would now be timely. Of particular concern are (1) control and management of the front end, such as clocking and labeling, (2) determination and application of calibration constants, (3) outputs needed for the trigger, (4) data processing needed and (5) test features.

In the area of off-detector data acquisition electronics, that is, high-speed busses, event builders, and microprocessor farms, much of the necessary development will occur naturally through implementation of on-line farms for existing experiments, such as CDF and D0. Some further R&D into high-speed busses and event builders is warranted.

The trigger processors will most likely depend on custom VLSI circuits for reasons of speed and the advantages of detector mounting. Consequently, R&D in this area is needed. The final designs will depend on, and help determine, details of system integration. Trigger circuits of certain usefulness include analog sum and discrimination circuits (including E_T sums), shower cluster finders, and track segment finders. Also of interest is the study of on-line track finders using specialized, fully-custom, or general-purpose processors.

10.7. Detector Simulation

Computer simulation of the components of the Large Solenoid Detector and of the detector as a whole will be a very important part of the design of the detector. The ratio of events from interesting physics to events from background processes is very low, so detailed understanding of detector response to the backgrounds is needed. Any large detector for the SSC will be very complex and expensive and every effort must be made to design a detector which will have excellent performance and will not have to undergo major rebuilding. Some areas in which computer simulation is particularly needed are pattern recognition in tracking detectors, discussed in previous sections, and development of shower simulation code which can be trusted as an aid in the design and optimization of the calorimeter, including its electron identification performance. Existing codes require too much computer time to be practical and need to be compared with test beam data at energies of several hundred GeV. Computer simulation of the processing of the data, including electronics response to the signals from the detector components, processing of the data by microprocessors on the detector, trigger, and data acquisition will be required.

11. Conclusions

The physics at the SSC will require high resolution hermetic calorimetry and excellent electron and muon identification. These needs are met by the large solenoid detector discussed here. Hermetic calorimetry is obtained in the presence of a magnetic field by placing the entire unit inside the solenoid coil. Good momentum resolution in the tracking has been preserved by choosing a 2 Tesla magnetic field (although moderately lower fields would not substantially change the performance of the detector). Some thought has been given to intermediate angle tracking although the designs outlined are very preliminary. Electron identification with a pion misidentification probability of less than 10^{-3} can be obtained with only calorimetry and conventional tracking. This meets the goals outlined by the physics study groups. However, there was a strong feeling that better rejection than this should be provided if possible; some kind of TRD system, integrated with the tracking, is a likely candidate. The solenoid coil, 8 meters in diameter and 16 meters long, has been designed in cryogenically separate modules for ease of construction and to allow access to the calorimetry. The large integral $B\,d\ell$ of the solenoid (8 Tesla-meters) allows adequate momentum resolution for muons to 1–2 TeV/c and charge sign measurement to momenta exceeding 5 TeV/c.

The design parameters of the proposed detector are summarized in Table X.

Table X. Summary of the Detector Design Parameters

SOLENOID COIL	
Inner diameter	8.2 meters
Length	16 meters
Central field	2 Tesla
Weight (including flux return)	16,450 metric tons
CENTRAL TRACKING	
Inner radius	0.40 meters
Outer radius	1.6 meters
Number of superlayers	15
Number of cells	122,368
$|\eta|$ coverage	< 1.2
INTERMEDIATE TRACKING (OPTIONS A & B)	
$|\eta|$ coverage	$1.2 < |\eta| < 3.0$
z position	$|z| < 4.0$ meters
Total number of chambers	26 (A) or 18 (B)
Total anode wires	128,000 (A) or 172,800 (B)
Total cathode pad channels	500,000 (A) or 293,760 (B)
ELECTROMAGNETIC CALORIMETER	
Depth	25 X_0
Transverse segmentation	$(\Delta\eta \times \Delta\phi)$
$|\eta| < 2.0$	$.02 \times .02$
$2.0 < |\eta| < 4.5$	$.03 \times .03$
$4.5 < |\eta| < 5.5$	$.03 \times .03$ to $.08 \times .08$
Longitudinal segmentation	6 X_0, 8 X_0, 11 X_0
Total number of towers	104,000
Total number of electronics channels	312,000
Weight	
Central	200 metric tons
Forward	35 metric tons
HADRONIC CALORIMETER	
Depth	10–12 λ
Transverse segmentation	$(\Delta\eta \times \Delta\phi)$
$|\eta| < 2.0$	$.06 \times .06$
$2.0 < |\eta| < 4.5$	$.06 \times .06$
$4.5 < |\eta| < 5.5$	$.06 \times .06$ to $.08 \times .08$
Longitudinal segmentation	2 segments
Total number of towers	19,100
Total number of electronics channels	37,200
Weight	
Central	4800 metric tons
Forward	965 metric tons
MUON SYSTEM	
Total number of electronic channels	$\sim 100,000$
Weight of toroids	13,000 metric tons

A very substantial amount of R&D must be performed if the detector is to be optimally and efficiently constructed, and specific R&D areas were identified and discussed in the preceding section. In addition to basic research and development, prototype work must be done on all components of the detector. The choice of sampling medium for the calorimeter is especially critical, but testing is needed for all aspects of the design, partly because of the scale of the construction task. However, it is believed that the amount of R&D required is consistent with the length of time available so that the detector can be built and ready at the turn-on of the SSC.

Relatively little time was spent at this Workshop discussing the problems of electronics, triggering, rate and pile-up effects, and data handling and analysis. For some of these subjects reasonably careful studies were performed during Snowmass 1986 (or at previous workshops), but all require further study and must be brought under control in the early stages of detector design.

In spite of the rather large amount of R&D which remains to be done, there was considerable optimism that there are no fundamental obstacles to the design, construction, and operation of a detector with the excellent detection of electrons, muons, jets, and missing energy that is required for analyzing the exciting physics that awaits at 40 TeV.

References

1. Proceedings of the 1984 Summer Study on the Design and Utilization of the Superconducting Super Collider, edited by R. Donaldson and J. G. Morfin, Snowmass, CO (1984).

2. Cost Estimate of Initial SSC Experimental Equipment, SSC–SR–1023, SSC Central Design Group, June 1986.

3. Proceedings of the 1986 Summer Study on the Physics of the Superconducting Supercollider, edited by R. Donaldson and J. Marx, Snowmass, CO (1986).

4. See the Reports of the Parametrization Subgroups in these Proceedings.

5. K. Tsuchiya *et al.*, KEK Preprint 86-63, October 1986.

6. T. Kondo, "Report of the Microvertex Detector Group," Proceedings of the 1986 Summer Study on the Physics of the Superconducting Supercollider, edited by R. Donaldson and J. Marx, Snowmass, CO (1986), p. 743.

7. D. G. Cassel and G. G. Hanson, "Report of the Central Tracking Group," *ibid.*, p. 377.

8. R. DeSalvo, "A Proposal for an SSC Central Tracking Detector," *ibid.*, p. 391.

9. D. H. Saxon, "Vertex Detection and Tracking at Future Accelerators," Proceedings of the Workshop on Future Accelerators at High Energies, La Thuile/CERN (1987), RAL 87–011.

10. E. Elsen and A. Wagner, "Tracking Detectors for Large Hadron Colliders and for e^+e^- Linear Colliders," *ibid.*

11. R. L. Gluckstern, Nucl. Instr. and Meth. **24**, 381 (1963).

12. R. DeSalvo, "A Proposal for an SSC Central Tracking Detector," CLNS 87/52.

13. M. Atac, T. Hessing and F. Feyzi, IEEE Trans. Nucl. Sci. **33**, 189 (1986).

14. H. A. Gordon and P. D. Grannis, "Calorimetry for the SSC," Proceedings of the 1984 Summer Study on the Design and Utilization of the Superconducting Super Collider, edited by R. Donaldson and J. G. Morfin, Snowmass, CO (1984), p. 541.

15. T. Kondo, H. Iwasaki, Y. Watanabe, and T. Yamanaka, "A Simulation of Electromagnetic Showers in Iron-, Lead-, and Uranium–Liquid Argon Calorimeters Using EGS and Its Implications to e/h Ratios in Hadron Calorimetry," ibid., p.556.

16. R. Partridge, "Calorimeter Requirements for Tagging the Semi–Leptonic Decays of Top Quarks," ibid., p. 567.

17. E. Fernandez et al., "Identification of W Pairs at the SSC," ibid., p. 107.

18. T. Akesson et al., "Detection of Jets with Calorimeters at Future Accelerators," Proceedings of the Workshop on Future Accelerators at High Energies, La Thuile/CERN (1987), CERN/EP/87-88.

19. G. Brandenburg et al., "Identification of Electrons at the SSC," Proceedings of the 1986 Summer Study on the Physics of the Superconducting Supercollider, edited by R. Donaldson and J. Marx, Snowmass, CO (1986), p. 420.

20. P. Jenni et al., "Report of the Jet Group," Proceedings of the Lausanne Workshop on the LHC.

21. R. Wigmans, CERN-EP/86–141 (1986), submitted to Nucl. Instr. and Meth. See also the references contained therein.

22. C. Baltay, J. Huston, and B. G. Pope, "Calorimetry for SSC Detectors," Proceedings of the 1986 Summer Study on the Physics of the Superconducting Supercollider, edited by R. Donaldson and J. Marx, Snowmass, CO (1986), p. 355.

23. S. R. Hahn et al., "Calibration Systems for the CDF Central Electromagnetic Calorimeter," submitted to Nucl. Instr. and Meth., August 1987.

24. Technical Proposal for Aleph, CERN/LEPC/83-2, LEPC/P1 (1983).

25. T. J. Devlin, A. Lankford, and H. H. Williams, "Electronics, Triggering, and Data Acquisition for the SSC," Proceedings of the 1986 Summer Study on the Physics of the Superconducting Supercollider, edited by R. Donaldson and J. Marx, Snowmass, CO (1986), p. 439.

26. A. Gonidec et al., Proceedings of the International Conference on Advances in Experimental Methods for Colliding Beams, March 9–13, 1987, Stanford, California, to be published in Nucl. Instr. and Meth.

27. W. Wenzel, D0 Internal Note #524, Fermilab.

28. V. Radeka, "Fundamental Limits on Ionization Calorimetry," Proceedings of the International Conference on Advances in Experimental Methods for Colliding Beams, March 9–13, 1987, Stanford, California, to be published in Nucl. Instr. and Meth.

29. J. Engler and H. Keim, Nucl. Instr. and Meth. **223**, 47 (1984).

30. H. H. Williams, "Detector Summary Report", Proceedings of the 1986 Summer Study on the Physics of the Superconducting Supercollider, edited by R. Donaldson and J. Marx, Snowmass, CO (1986), p. 327.

31. L. Nodulman et al., Nucl. Instr. and Meth. **204** 351 (1983).

32. Report of the Task Force on Detector R&D for the Superconducting Super Collider, SSC–SR–1021, SSC Central Design Group, June 1986.

33. R. Engelmann *et al.*, Nucl. Instr. and Meth. **216**, 45 (1983).

34. B. Dolgoshein, Nucl. Instr. and Meth. **A252**, 137 (1986).

35. D. Carlsmith *et al.*, "SSC Muon Detector Group Report," Proceedings of the 1986 Summer Study on the Physics of the Superconducting Supercollider, edited by R. Donaldson and J. Marx, Snowmass, CO (1986), p. 405.

36. Proceedings of the Workshop on Triggering, Data Acquisition and Offline Computing for High Energy High/High Luminosity Hadron–Hadron Colliders, edited by B. Cox, R. Fenner and P. Hale, Fermilab, Batavia, IL (1985).

37. G. Kane, F. Paige, L. Price *et al.*, "SSC Physics Signatures and Trigger Requirements," *ibid.*, p. 1.

38. A. J. Lankford and G. P. Dubois, "Overview of Data Filtering/Acquisition for a 4π Detector at the SSC," *ibid.*, p. 185.

39. P. Cooper *et al.*, "A Feasibility Design for the Readout of a 4π SSC Detector," *ibid.*, p. 200.

40. T. J. Devlin, A. Lankford, and H. H. Williams, "Electronics, Triggering, and Data Acquisition for the SSC," Proceedings of the 1986 Summer Study on the Physics of the Superconducting Supercollider, edited by R. Donaldson and J. Marx, Snowmass, CO (1986), p. 439.